Fachhochschule Aachen, Campus Jülich

Fachbereich Energietechnik (FB 10)

Studiengang Physical Engineering (AOS)

Studienrichtung Produktentwicklung

Electrical resistance of the solder connections for the consolidation of the LHC main interconnection splices

Bachelorarbeit von Robin Lutum

Jülich, Deutschland

Dezember 2011

Diese Arbeit ist von mir selbstständig angefertigt und verfasst. Es sind keine anderen als die angegeben Quellen und Hilfsmittel benutzt worden.

Robin Lutum

Diese Arbeit wurde betreut von:

1. Prüfer: Prof. Dr. rer. nat. Arno Förster, Fachhochschule Aachen

2. Prüfer: Dipl. Ing. (FH) M.Sc. Christian Scheuerlein, CERN TE-MSC-SCD

Diese Arbeit wurde im Rahmen eines Aufenthalts im Technical Student Programme der European Organization for Nuclear Research (CERN) in Genf, Schweiz durchgeführt.

Zusammenfassung

Für die Konsolidierung der LHC-Hauptstromverbindungen ist es geplant Parallelwiderstände auf jede der 10.170 Verbindungsstellen zu löten. Für diese Aufgabe wurde Sn60Pb40-Lot ausgewählt. In diesem Kontext wurde der elektrische Widerstand der Überlappungsverbindung von Parallelwiderstand und Busbar im Temperaturbereich von Raumtemperatur bis 20 K gemessen. Ein Cryocooler-Aufbau wurde adaptiert, um eine Widerstandsmessung im niedrigen nΩ-Bereich mit bis zu 150 A Messstrom durchführen zu können. Um den Einfluss des Widerstandes der Lotschicht auf den Gesamtwiderstand der Verbindung zu untersuchen wurden außerdem Verbindungen mit Sn96Ag4- und Sn77.2In20Ag2.8-Lot vermessen. Der Einfluss des Sn60Pb40-Lotschichtwiderstands ist vernachlässigbar bei einer Messung des Gesamtwiderstands über eine Länge von 6 cm längs der Verbindung. Bei einer transversalen Messung wird der Gesamtwiderstand signifikant vom Lotschichtwiderstand beeinflusst. Die mit Sn77.2In20Ag2.8-Lot hergestellten Verbindungen zeigen signifikant höhere Widerstandswerte, wie durch den hohen spezifischen Widerstand des Lotes bei kryogenischen Temperaturen zu erwarten.

Abstract

For the consolidation of the LHC main interconnection splices it is planned to solder shunts onto each of the 10,170 splices. The solder that has been selected for this purpose is Sn60Pb40. In this context the electrical resistance of the shunt to busbar lap splices has been measured in the temperature range from RT to 20 K. A cryocooler setup has been adapted such that a test current of 150 A can be injected for accurate resistance measurements in the low nΩ range. In order to study the influence of the solder bulk resistivity on the overall splice resistance, solder connections produced with Sn96Ag4 and Sn77.2In20Ag2.8 solder have been studied as well. The influence of the Sn60Pb40 solder resistance is negligible when measuring the splice resistance in a longitudinal configuration over a length of 6 cm. In a transverse measurement configuration the splice resistance is significantly influenced by the solder. The connections prepared with Sn77.2In20Ag2.8 show significantly higher resistance values, as expected from the relatively high solder resistivity at cryogenic temperatures.

Contents

1. Introduction

The Large Hadron Collider (LHC) [1] at the European Organization for Nuclear Research (CERN) is the world's largest particle accelerator. It is located in a 27 km long underground tunnel beneath the franco-swiss border near Geneva, Switzerland. The LHC is designed to accelerate two counter-rotating beams of Hadrons up to a centre of mass energy of 7 TeV (in the case of Protons that are obtained by stripping electrons from Hydrogen atoms) or 2.76 TeV/u (energy per nucleon, in the case of Lead ion acceleration).

In a circular collider the maximum particle energy is proportional to the collider's radius and to the magnetic field of the dipole bending magnets that keep the particle beam on its circular path (and consequently to the electrical current flowing through the coils of these dipole electromagnets). With its 27 km circumference the LHC fulfils one requirement for high energy collisions, the radius. The other requirement, magnetic field strength, is achieved by using superconducting cables for coil construction in the 1,232 bending dipoles of the machine. The dipole coils are wound from superconducting cable made of Niob-Titanium filaments [2]. The dipole coils are contained within the 15 m long cryo-dipoles, a schematic of which is shown in Figure 1. The magnetic fields of these dipole magnets are designed to exert a force on the particle bunches that rotate clockwise in one of the beam-pipes, and anticlockwise in the other.

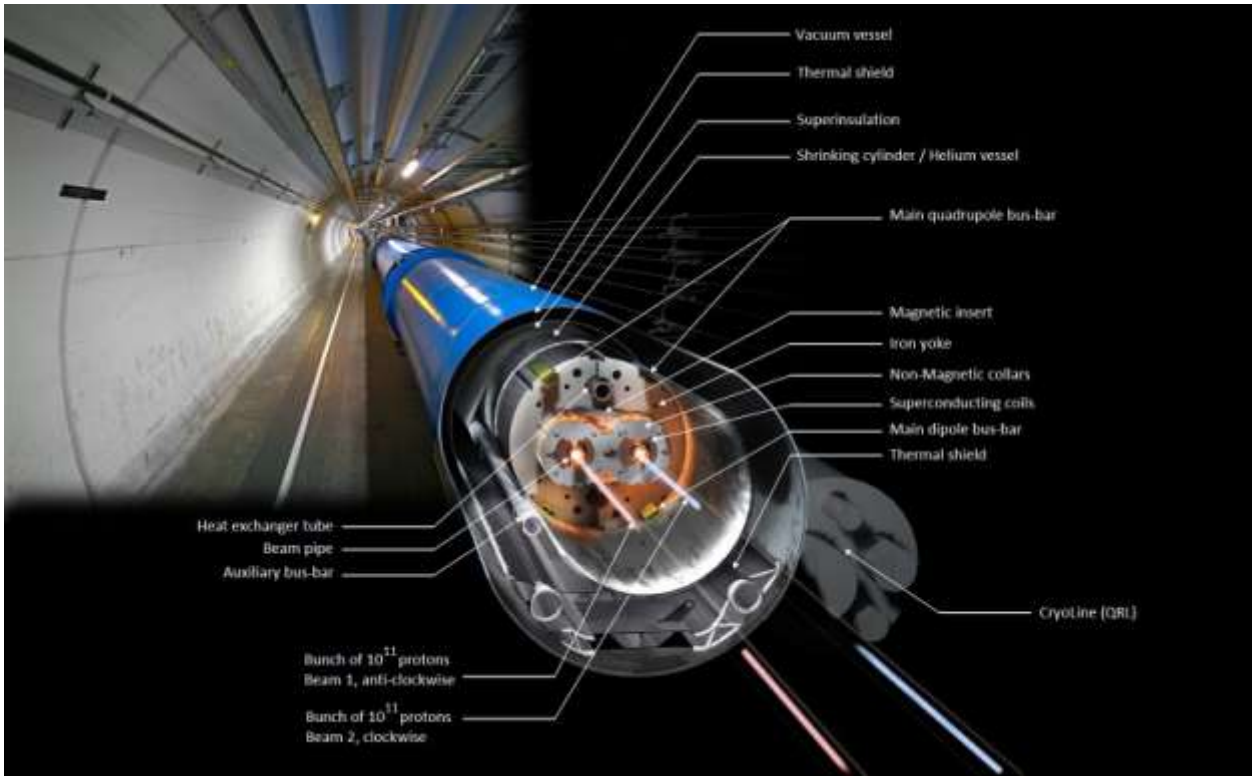

Figure 1: Schematic of the inside of a cryo dipole of the LHC. Modified by R. Lutum.

The LHC receives particles with an injection energy of 0.45 TeV from the accelerator-complex at CERN. At this point the magnetic field strength in the dipoles is 0.54 T, corresponding to 763 A

current in the coils. During the acceleration of the particles via radio-frequency cavities the magnetic field strength has to be increased proportional to the particle energy. At design energy of 7 TeV per beam (14 TeV collision energy) the nominal magnetic field strength of the dipole bending magnets is 8.3 T, which corresponds to a coil current of 11,850 A [3].

The LHC is organised in 8 sectors of equal size. The 154 dipole magnets in a sector are electrically connected in series, and powered by one power supply through busbars [4], which consist of a Nb-Ti/Cu superconducting cable and an additional Cu stabiliser. This requires low-resistance connections of the busbar cable and stabiliser between each dipole. A picture of an LHC main interconnection splice is shown in Figure 2 (a). Visible are the busbars on the left and right, and the two superconducting cables extending from the middle of these. Figure 2 (c) shows a schematic of how the interconnect is produced. The superconducting cables are made to overlay each other in an area of 120 mm and then inserted into a u-shaped copper profile. The top of this is closed with a flat copper wedge. Between each layer of this interconnection a foil of Sn96Ag4 solder is inserted. A force of 2.7 t is then applied to the connection with a hydraulic jack, and the solder is melted with an inductive soldering machine. After the soldering the cross section of the interconnection is similar to that of the busbar seen in Figure 2 (b). These superconducting splices are specified to have a resistance below 0.6 nΩ at 1.9 K [5].

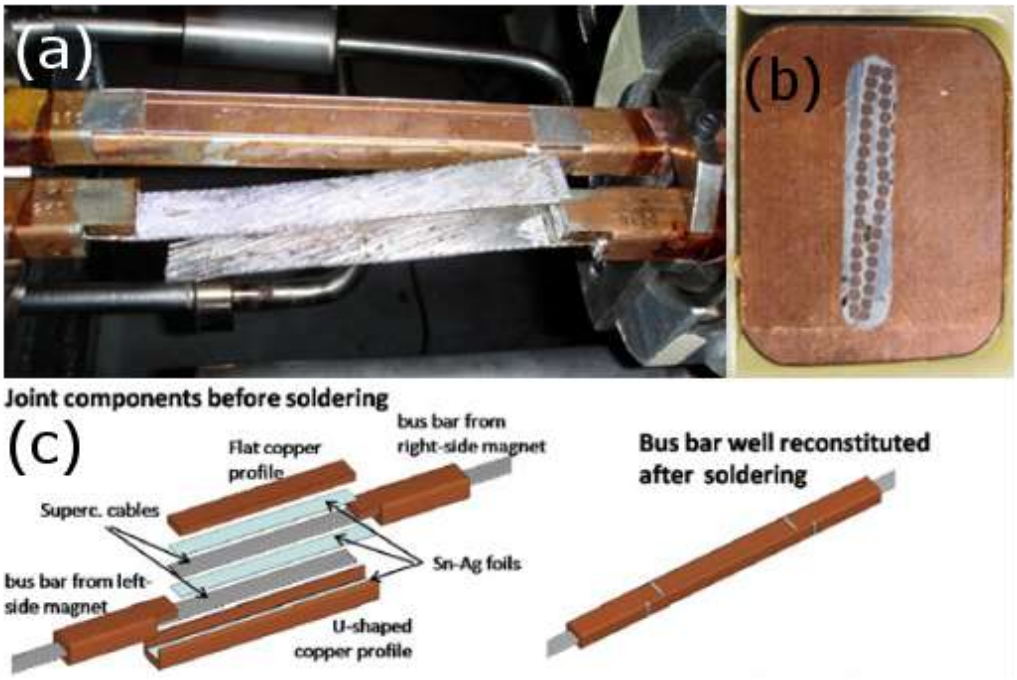

Figure 2: (a) Front: Two superconducting cables ready for splice. Back: Finished busbar splice. (b) Dipole busbar cross-section. (c) Schematic of the inter-dipole solder connection [6].

An excessive resistance, most likely in the splice between the two superconducting cables that connects the dipole busbars, is at the origin of the incident in September 2008 that caused a breakdown of the LHC and massive collateral damage to the accelerator [7]. The high resistance

caused a quench[1] of the splice and, due to lack of electrical and thermal contact between the cables and the copper stabilizer, and between the busbar stabilizer and the splice copper profiles, this resulted in a thermal run-away [8].

In case of a quench of the superconducting cable, in a sound splice, the current can safely be carried by the copper stabiliser for at least the time that it takes to drain the energy from the magnet coils (~104 s). If however the thermal and electrical contact between the superconducting cable and the busbar stabiliser, and between the busbar and the interconnection copper, is not sufficient, a thermal runaway can quickly happen, possibly reaching melting temperatures within seconds.

During the 2008-2009 LHC shutdown the room-temperature (RT) resistance of about 230 LHC splices has been measured. From these local resistance measurements it is estimated that ~15% of the about 10,000 main interconnection splices exhibit too much excess RT resistance and require a consolidation before the machine can be commissioned for 7 TeV. During the shutdown foreseen for 2013 it is planned to repair all splices with too high excess resistance. In addition it is planned to add shunts to all of the splices in order to guarantee a redundant current path in the non-superconducting state for all LHC main busbar interconnection splices. These shunts will be soldered on the top and on the bottom of the dipole busbar-to-splice contact surface and on the bottom of the quadrupole splice connections. The shunts can act as an alternative route for the current during a magnet quench and subsequent magnet energy discharge. A drawing of the current shunt design can be seen in Figure 3 [9].

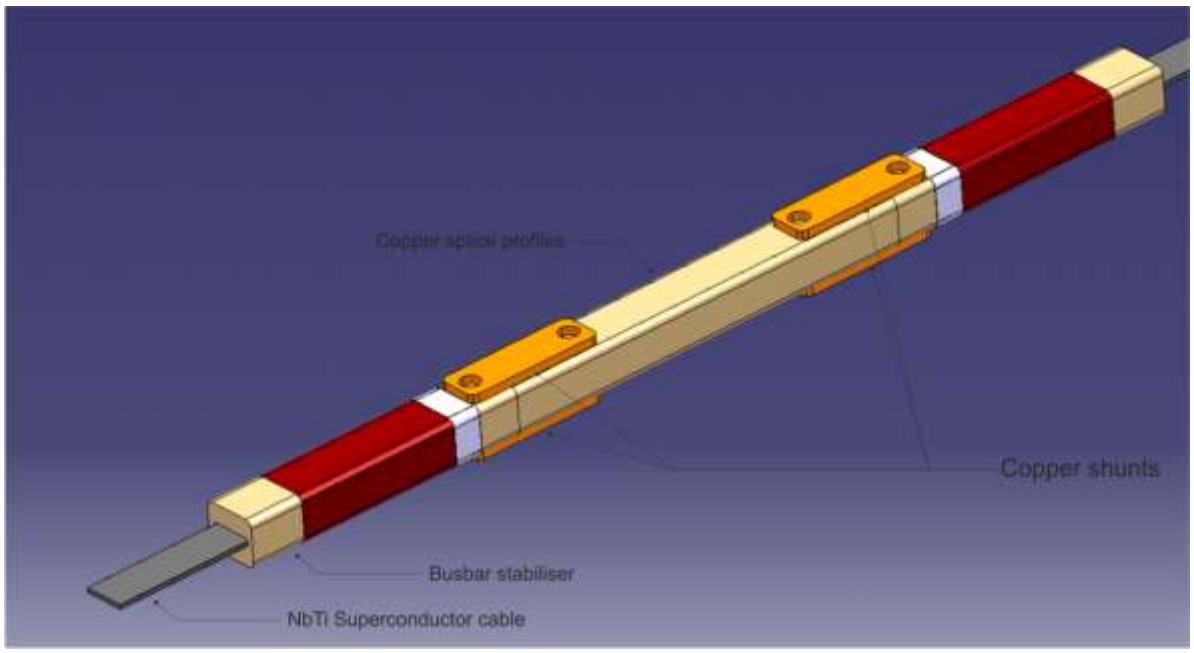

Figure 3: Drawing of a consolidated LHC dipole main interconnection splice with soldered shunts (courtesy P. Fessia, CERN).

The solder that has been chosen for the shunt to busbar stabiliser connections is the near eutectic Sn60Pb40, whose melting temperature of 183 °C is significantly lower than the Sn96Ag4 melting

[1] Quench: Sudden transition from superconducting to normal conducting state in a superconductor

temperature of 221 °C. This allows soldering of the shunt to the splice stabiliser, without melting the existing Sn96Ag4 connections.

The goal of this work is to characterise the electrical resistance in the approximate temperature range from RT to 20 K of solder lap splices, consisting of a shunt soldered to a quadrupole busbar, in order to study the influence of the solder alloy on the overall splice resistance. The lap splices were produced with Sn60Pb40 solder (currently foreseen for the consolidation), Sn96Ag4 solder (used in the interconnections) and Sn77.2In20Ag2.8 solder (high resistivity solder for comparison). Furthermore a batch of butt splices with well defined Sn60Pb40 solder thickness was produced and characterised by resistance measurements and tensile tests.

To conduct the experiment a cryocooler setup was modified for variable temperature resistance measurements in the low nΩ range with test currents up to 150 A. With a cryocooler, which uses a closed Helium cycle to provide refrigeration, it is comparatively easy to control the sample temperature over a wide range. However, the drawback of a cryocooler is the limited cooling power, as compared to refrigeration systems relying on liquid or gaseous Helium in direct contact with the sample. Thus, the cryocooler setup requires careful design, especially of current leads and measurement instrumentation, in order to minimise the heat-load for a given temperature. The adaptation of the experimental set-up for low resistance measurements and its characterisation are therefore a crucial part of the work performed in the context of this thesis.

2. Experimental

2.1. The original cryocooler setup

An existing cryocooler setup (so-called Rial Special Cryostat), which is used for thermal contraction measurements in a temperature range from RT to approximately 10 K, was modified for electrical resistance measurements at cryogenic temperatures. Figure 4 (a) shows the cryocooler setup in its original configuration. From bottom to top the picture shows:

- The aluminium frame holding the components of the setup (below the table are vacuum pump, temperature monitor, electrical switchbox)
- The support-structure holding the lower part of the vacuum chamber and the Cryodyne Refrigeration System (latter not visible)
- The lower vacuum chamber with four DN25 flanges for instrumentation and vacuum connections
- The upper vacuum chamber with four Quartz windows for the length measurement using a laser measurement system

Figure 4 (b) shows the inside of the cryostat setup for thermal contraction measurements. A denotes the first stage of the Cryodyne Refrigeration System, B the second stage (also referred to as "coldhead"). The sample whose thermal contraction is to be measured can slide over the sample holder. C points to the two temperature probes mounted on the sample, which measure the temperature at both ends of the sample.

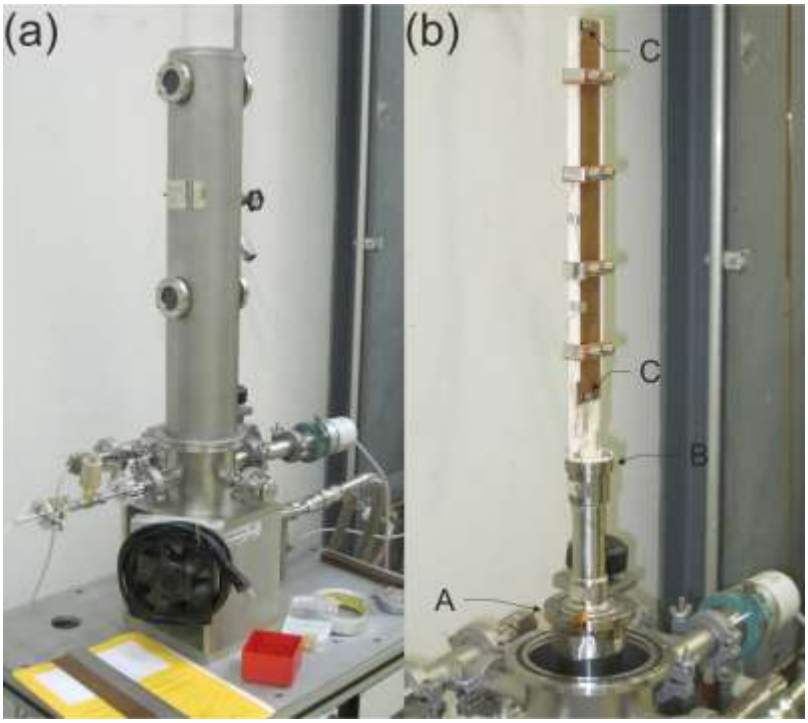

Figure 4: (a) Cryocooler with cryostat for thermal-contraction-measurements. (b) Sample holder for thermal contraction measurements.

2.2. The cryocooler setup modified for electrical resistance measurements in the nΩ range

Since the resistance of the high purity Cu splices to be studied at cryogenic temperature is very low (in the order of 5 nΩ for R_trans of the lap splices), a high test current of 150 A is needed to obtain a sufficiently high voltage signal. The cryocooler setup requires the following modifications:

- A dedicated sample holder providing good thermal contact between sample and coldhead, the ability to mount different samples geometries and space for instrumentation and thermalisation
- Installation of a new heat-shield to protect against heat-input from radiation
- Installation of a new vacuum vessel of sufficient size to contain the adaptations
- Instrumentation for potential measurement
- Installation of 150 A current leads with minimised heat input
- Installation of heaters to regulate the temperature and characterise the cryocooler performance

Figure 5 shows this setup. The Helium compressor with the heater power supply and multimeter for heater voltage are shown on the left. The Nitrogen bottle in the back is used for vacuum purging. On the right is the power supply for the measurement current, two multimeters for voltage measurement, an auxiliary multimeter and an auxiliary power supply. In the middle the cryostat is visible on its support table, which also holds the temperature monitor, the vacuum pump and the vacuum monitor.

Figure 5: The modified cryocooler setup.

2.2.1. Refrigeration system

The closed-cycle refrigeration system of the cryocooler consists of a CTI-Cryogenics Cryodyne Refrigeration System Model 350 connected to a CTI-Cryogenics Model 8200 Helium Compressor. The functional principle is essentially similar to that of a common household refrigerator. Since the working fluids used in non-cryogenic applications solidify below a certain temperature (e.g. Haloalkane R-134a, melting point -101° C at 1.013 bar [10]), a working fluid with a lower melting point must be used. In the case of the cryocooler this is Helium. It is compressed and the heat of compression is removed with an air-cooled heat exchanger. This compressed Helium gas is then transported to the refrigeration unit. To achieve the extremely low temperatures the Cryodyne Refrigeration System, different from its household counterparts, uses a so-called regenerator in the helium path (see Figure 6 (a)). The Helium is then cycled through the following way [11]:

- Valve A opens and compressed Helium gas enters the area above the displacer at RT. The displacer with the integrated regenerator is at the bottom position.
- The displacer is moved upwards via a motor and crankshaft assembly. The Helium passes through the regenerator matrix, which absorbs heat from the Helium gas. The gas temperature is close to that of the load now.
- Valve A closes and valve B opens. The Helium gas is allowed to expand lowering its temperature. Heat is transferred from the load to the gas.
- The expanding gas passes through the regenerator absorbing heat energy from it.
- The displacer moves downwards, forcing the remainder of the cool gas out of the lower cylinder through the regenerator matrix.
- The low pressure gas leaves the refrigeration unit through valve B at approximately RT. It is transported back to the compressor and the cycle starts again.

Figure 6 (b) shows the configuration of the Cryodyne Refrigeration System Model 350 used in this experiment. Two stages are cascaded behind each other in the Helium path to achieve refrigeration down to 6 K. A single-stage refrigerator could provide refrigeration in the 30–77 K range.

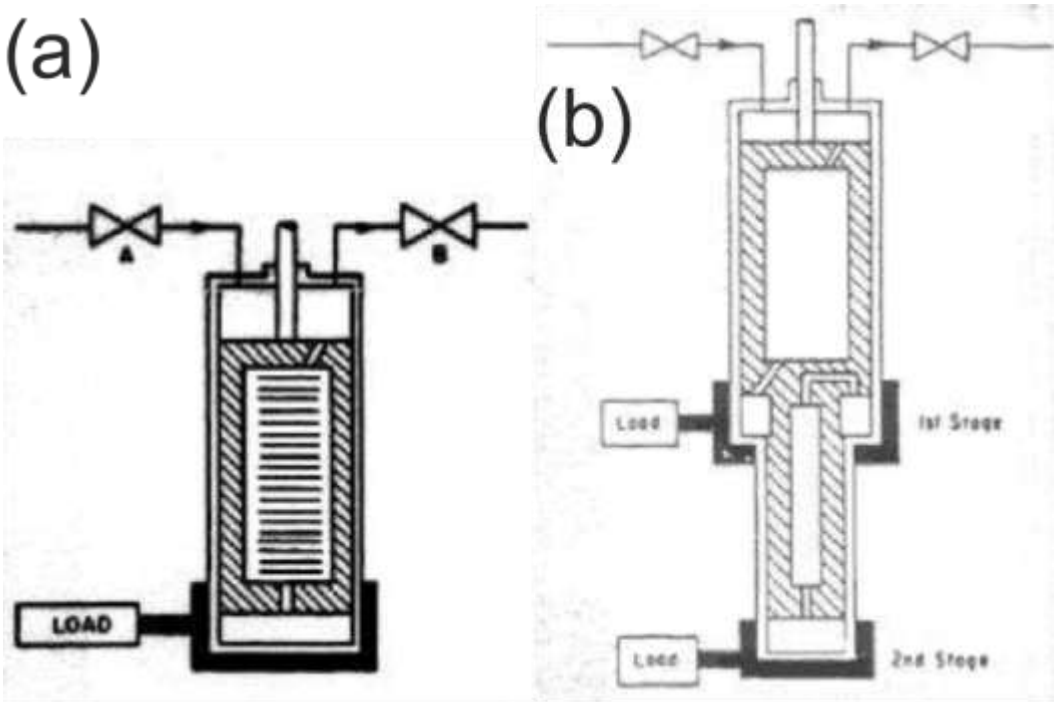

Figure 6: (a) Schematic of single-stage refrigeration unit. (b) Schematic of the two-stage refrigeration unit [11].

2.2.2. Vacuum pump and gauge

Vacuum is created by an oil-sealed dual rotary-vane mechanical vacuum pump (Alcatel Pascal 2021 SD). The vacuum pump is kept running until the pressure is approximately 2 x 10^{-2} mbar. The vacuum pump is then switched off and a further reduction in pressure is achieved by cryopumping[2]. At 23 K sample temperature the final pressure in the vacuum system is typically 5 x 10^{-3} mbar. The pressure is sensed by a Pfeiffer Compact full range gauge Typ PKR 251 that is read out by a Pfeiffer Typ TPG 252 A Dual sensor Vacuum Monitor.

2.2.3. Temperature measurement

For temperature measurements in the cryostat four DT-470/471CU Silicon Diode Temperature sensors are available. They are designed for temperature measurements in the range of 1.4-325 K. For readout and data-acquisition the probes are connected to a LakeShore Model 218 Temperature Monitor. The tolerance band of these diodes is ±0.5 K from 2-100 K and ±1 K from 100-305 K.

[2] Cryopumping: condensation of vapours and gases on a surface of low temperature.

2.2.4. Sample holder

The bare sample holder can be seen in Figure 7 (a). It is made of anodised aluminium and attached to the coldhead of the refrigeration system with four No. 6 (imperial standard) screws. Between the coldhead and the sample holder there is a compressed layer of 99.9% Indium wire to guarantee good thermal contact. To be able to mount samples of various dimensions and shapes there are two long holes along the mounting surface of the sample holder. The sides of the sample holder offer space for thermalisation of the current leads, the temperature probe wires and the voltage-measurement wires.

Figure 7 (b) shows a fully instrumented lap-splice sample mounted on the sample holder. It is clamped to the sample holder with one M5-screw visible on the top below the top current input. Also visible is the left thermalisation block, with two Cu-wires clamped to the Cu-block on the top, and two Cu-wires connecting the thermalisation block to the sample. Figure 7 (c) shows a butt-splice sample mounted to the sample holder and ready for measurement. Due to the lower current requirement for the measurement of the butt-splice samples, only one Cu-wire is used on each side of the sample for current input.

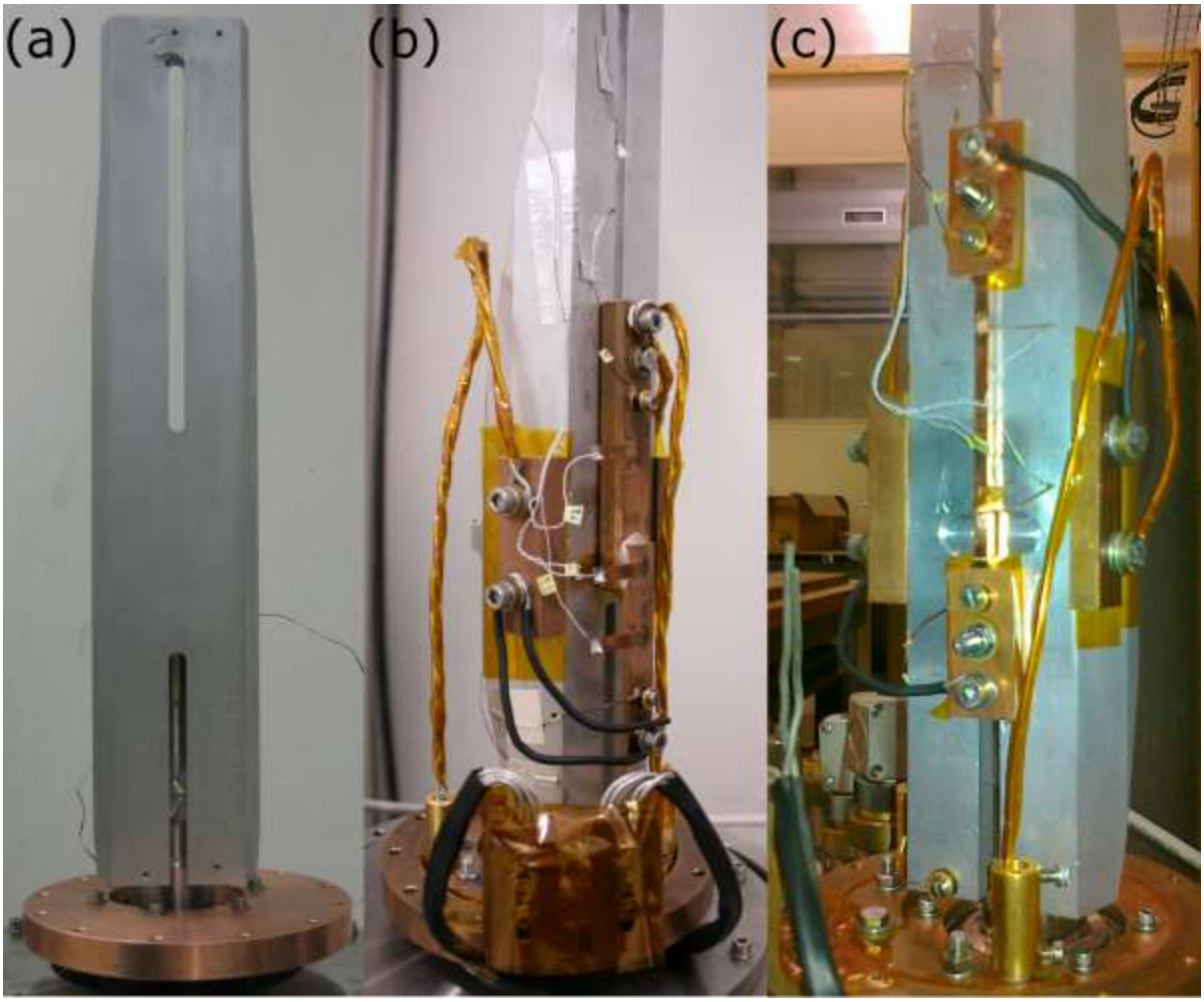

Figure 7: Sample holder with (a) no instrumentation or sample, (b) instrumented lap-splice sample with two Cu-wires per side for current input and (c) instrumented butt-splice sample with one Cu-wire per side for current input.

2.2.5. Cryostat and heat shield

A larger stainless-steel vacuum vessel is required in order to accommodate the sample holder, the sample and the current leads. The vacuum vessel with an inner diameter of 200 mm and a height of 564 mm is shown in Figure 8 (a). The stainless-steel disc that holds the vacuum vessel and the flutes for gaskets required for vacuum sealing, and the gasket sealing disc, are shown as well (Figure 8 (b) and (c)).

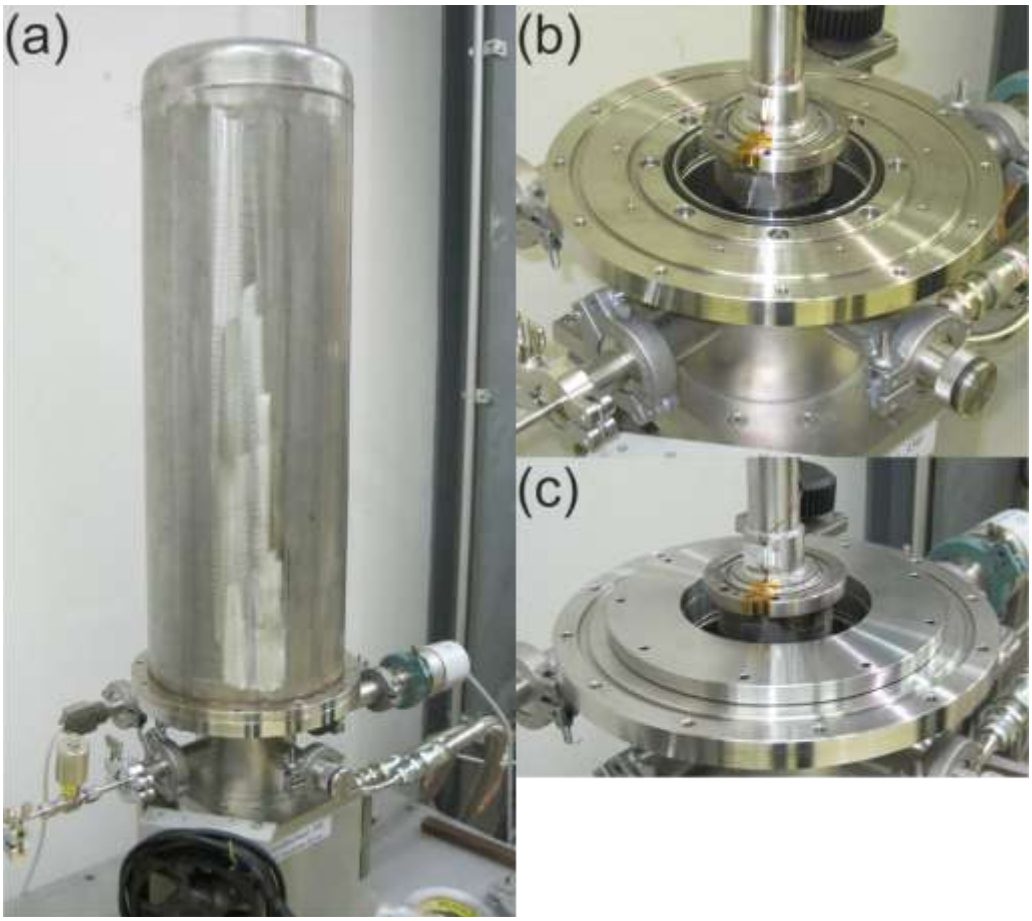

Figure 8: (a) The stainless-steel vacuum vessel. (b) Mounting disc for vacuum vessel. (c) Vacuum seal disc for vacuum vessel.

A heat shield between outer cryostat and the coldhead with the sample holder is kept at about 80 K in order to further reduce the heat input by radiation into the cryogenics-system. The heat shield consists of a copper tube of 100 mm inner diameter and of 461 mm inner height. The wall-thickness is 2mm. Figure 9 (a) shows the heat shield mounted on a 13 mm thick copper holding disc that is attached to the first stage of the cryogenics system.

The copper tube is coated with silver, which reflects heat radiation better than the copper surface. On the outside of the silver-coated copper tube multi layer insulation (MLI), so-called superinsulation, is installed. The MLI consists of several layers of Aluminium-coated polymer foils that are separated by layers of polyester net (tulle) or micro fibre glass fabric ("paper") [12]. The complete heat-shield assembly can be seen in Figure 9 (b).

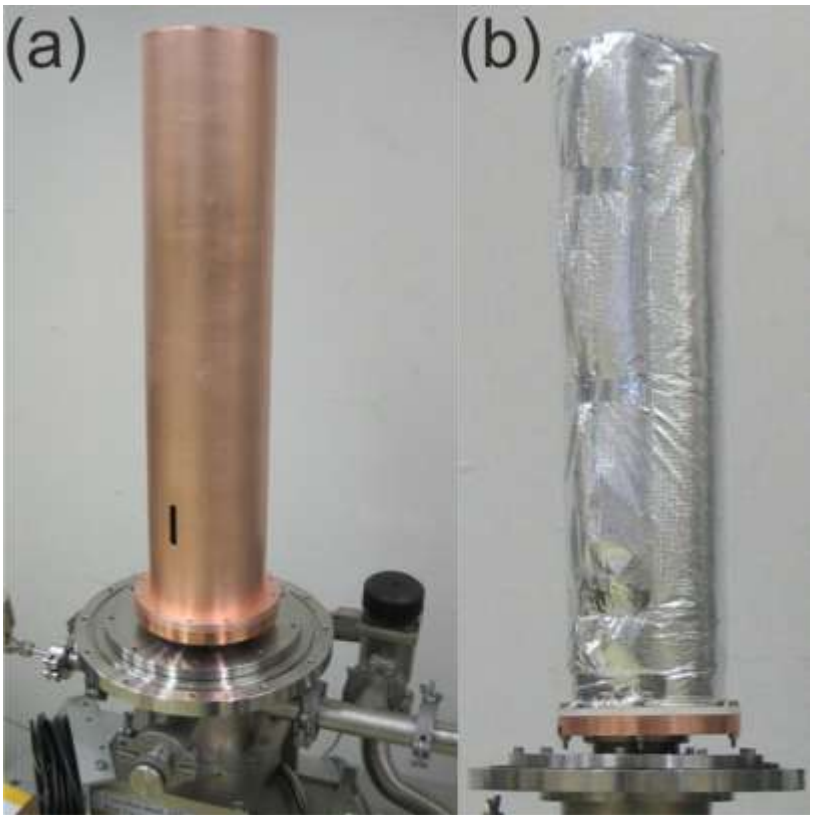

Figure 9: (a) Heat shield without coating and super insulation. (b) Heat-shield assembly with Multi Layer Insulation.

2.2.6. Current leads and other electrical connections

The current leads need to be designed in order to minimise the heat input into the cryogenic system by thermal conduction and Joule heating. The amount of heat input by thermal conduction is dependent on the conductor material, its cross-section, its length and temperature gradients within the conductor. The amount of heat input by resistive heating (Joule heating) is proportional to the conductor resistance and to the measurement current squared. For continuous operation the optimal conductor geometry is the one, in which the sum of heating due to conduction and of heating due to Joule heating is a minimum.

For measurements of the lap-splices with 150 A test current, the current leads from the feedthrough to the first stage of the cryocooler consist of five parallel 60 cm-long Cu wires with a diameter of 2 mm and a Residual Resistivity Ratio[3] (RRR) of 90. The wires are electrically insulated with heat shrinkable sleeves. The connection to the feedthrough is established with BeCu-Inline-Connectors from LewVac, UK. The connection from the first stage thermalisation to the sample is made with two parallel 30 cm-long Cu wires with 2 mm diameter and a RRR of 90.

[3] RRR: Ratio of RT resistivity to low-temperature resistivity (here 4.2 K)

For measurements of the butt-splices with 20 A test current, two of the five Cu-wires leading from feedthrough to the first-stage thermalisation are disconnected on the side of the first-stage thermalisation, and the number of leads per side from there to the sample is reduced to one Cu-wire.

The current feedthrough is the model ZFHP5-180C2-50KF-75 from LewVac, UK. This feedthrough has two copper conductors of 6.5 mm diameter that pass through a DN50KF fitting into the vacuum system. Figure 10 shows the current feedthrough and its mounting flange (right bottom and right top), as well as the current leads and the first-stage thermalisation. This feedthrough is rated at a maximum current of 180 A. It was chosen for the matching current range and the quick availability with custom dimensions (DN50KF flange instead of DN40KF, 75 mm vacuum-side conductors instead of 104.6 mm).

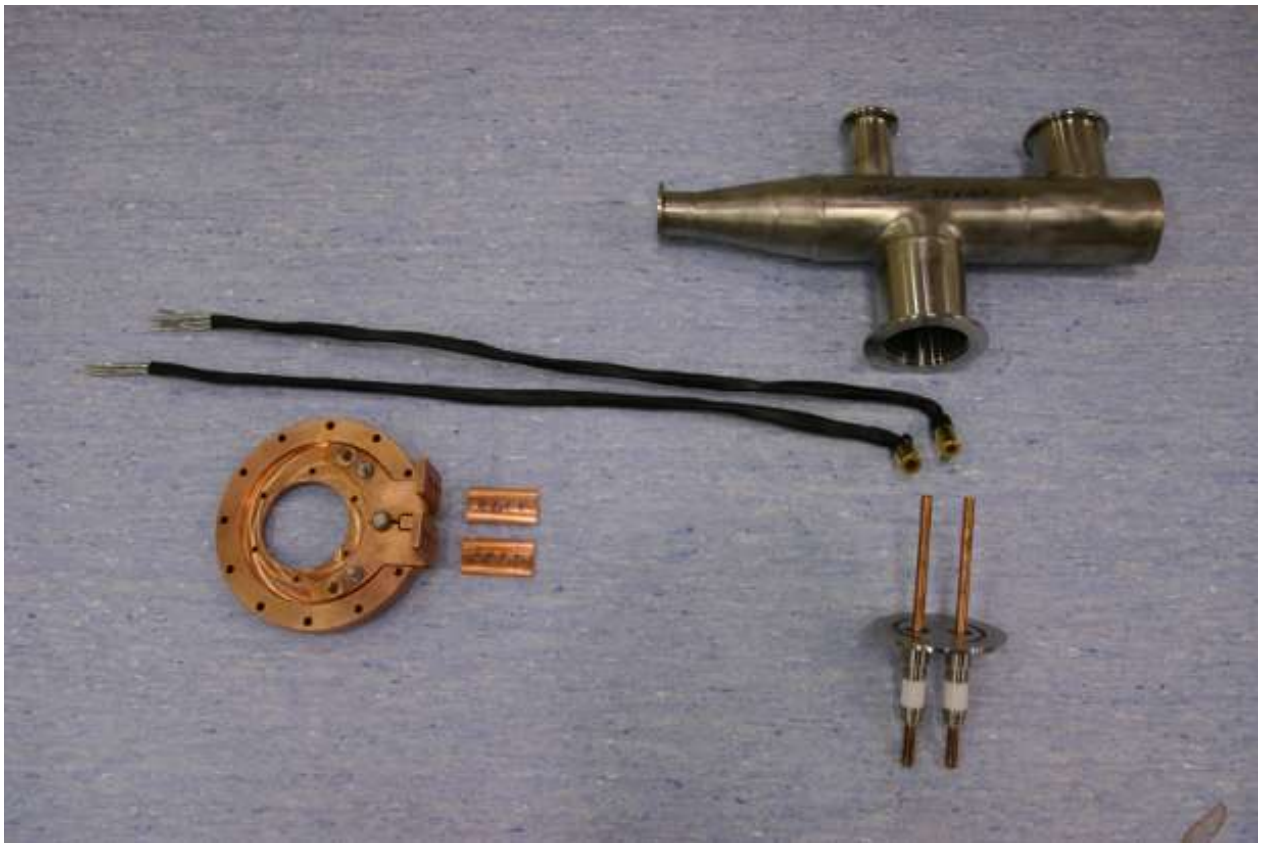

Figure 10: Flange for current feedthrough and vacuum instrumentation, first-stage current leads, first-stage thermalisation and current feedthrough

The thermal shield support disc was modified with a cut-out to accommodate copper pieces for a thermalised current feedthrough into the space enclosed by the heat shield. Figure 11 (a) shows the individual components of the thermalisation and feedthrough. From top to bottom the picture shows the heat-shield support disc, two BeCu-Inline-Connectors from LewVac UK, the two copper conductors, three plastic insulators for the machine screws and two copper mounting aids for the current leads coming from the current feedthrough.

Figure 11 (b) shows the fully-assembled feedthrough. The two copper conductors have adhesive Polyimide tape on the surfaces in order to electrically insulate both parts. The low thickness of the tape (approximately 50-70 µm) assures sufficiently good thermal contact.

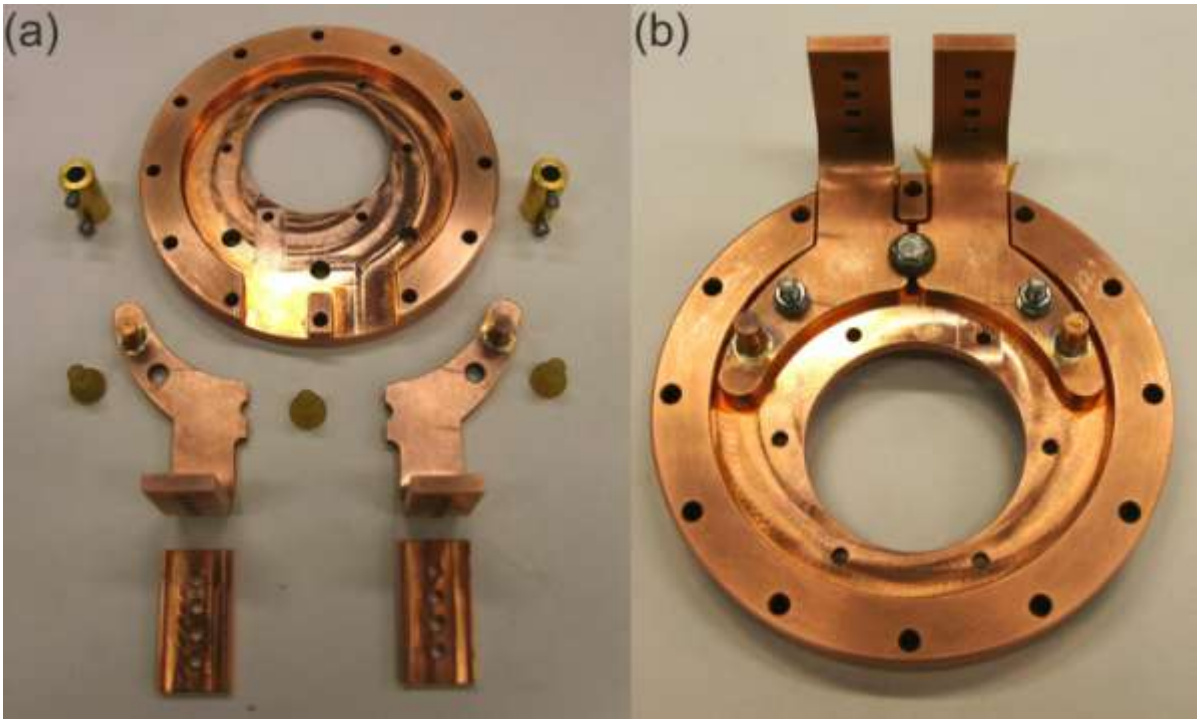

Figure 11: (a) Components and (b) assembly for first-stage thermalisation.

Figure 11 shows a fully instrumented lap-splice sample mounted on the sample holder. On the left behind the grey wires for voltage measurements, and on the right between the current leads, the first-stage thermalisation blocks are visible. They consist of copper blocks that are mounted to the sample holder with two M5-screws. The screws are insulated against the copper piece and the current leads with plastic spacers (as seen in Figure 11). Polyimide tape is applied between the sample holder and the copper blocks for electrical insulation. The two twisted Cu-wires arrive from the first-stage feedthrough and connect to the copper blocks. The current (and the heat-energy) then has to pass though the copper block before being connected to the sample with two short pieces of Cu wire.

The current leads are protected against a resistance runaway by limiting the maximum voltage of the current source to 1.1 V.

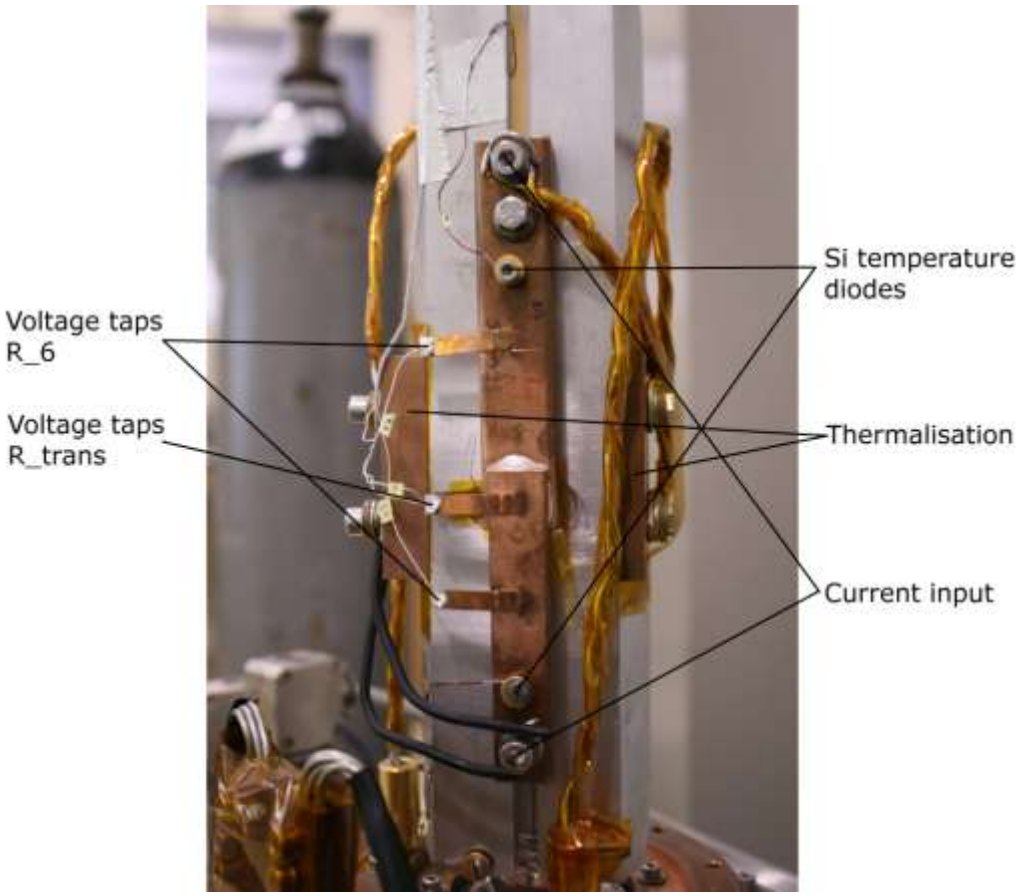

Figure 12: Mounted and instrumented solder sample and second-stage current-lead thermalisation.

To measure the voltage drop across the solder sample, four wires are routed from the sample to the digital multimeters outside the cryostat. For internal wiring synthetically insulated Cu-wire with a diameter of 0.1 mm was used.

An additional flange providing four twelve-pole Jaeger connectors is fitted to the purge valve flange at the lower jacket of the cryostat. One of the Jaeger connectors is used for the voltage measurement, while another one is used to supply electrical power to the heaters and to connect two of the temperature diodes to the temperature monitor.

2.2.7. Foil heaters

For temperature regulation and for validation the cryocooler performance two Minco foil heaters are attached to the two stages (HK5210R56.1L12A Thermofoil Heater 8.6 × 88.1 mm^2 for coldhead, HK5291R58.4L12 A Thermofoil Heater 19.8 × 25.4 mm^2 for first stage). The heaters are glued to the surfaces with Araldite two-component glue. Both heaters are backed with aluminium tape to prevent local hot-spots and to prevent heat radiation away from the cryocooler system.

The first-stage heater (Figure 13 (a)) is glued to the bottom of the thermal-shield mounting disc. After the cryocooler characterisation this heater was removed and the temperature regulation was performed with the coldhead heater only. The coldhead heater is wound around the collar of the coldhead. An aluminium disc of 30 mm diameter and 10 mm height is mounted on top of the coldhead to provide mounting space for the second temperature probe (Figure 13 (b)).

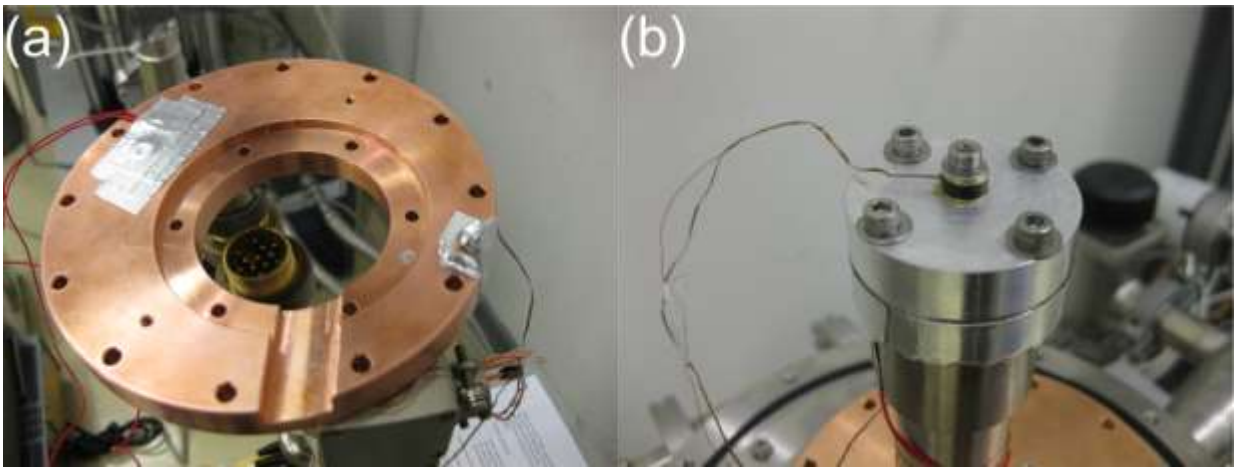

Figure 13: (a) First-stage heater on the bottom of the thermal-shield support disc (removed after cryocooler performance evaluation). (b) Coldhead heater and aluminium disc to hold temperature sensor.

2.3. Cryocooler performance evaluation

To be able to estimate the maximum allowable heat input through the current leads, it is necessary to know how much heat load can be dissipated by the two stages of the refrigerator while maintaining a certain temperature at the coldhead. This was achieved by independently heating the two stages of the cryocooler system with varying heating power using resistive foil heaters.

The electrical power to the heaters was supplied with a Thurlby Thandar Instruments PL330DP Dual power supply (TTi PL330DP) and with a Thurlby Thandar Instruments TSX1820P Programmable Power Supply (TTi TSX1820P). The voltage and current readings were performed with a Keithley DMM2000 Multimeter (DMM2000), a Keithley DMM2001 Multimeter (DMM2001) and a Hewlett-Packard 34401A Multimeter (HP 34401A).

For the individual measurements of the two stages, the two outputs of the TTi PL330DP were connected in series (U_{max} = 64 V, I_{max} = 3 A). The DMM2000 was used for the current reading, and the DMM2001 was used for the voltage reading.

The temperatures at first stage and coldhead were recorded for different power levels, once the temperatures had stabilised. The results for first stage heating can be seen in Figure 14. The graph shows the coldhead and first stage temperature as a function of heating duration at three different power levels. The waiting duration at constant heating power was chosen such that a temperature plateau was approached, although a stable temperature was not achieved in all cases. The scatter of the coldhead temperatures around an average is a result of the cyclic operation of the cryogenic system. The temperature is sampled at different points in the Helium cycle, and thus oscillates between a maximum and a minimum value.

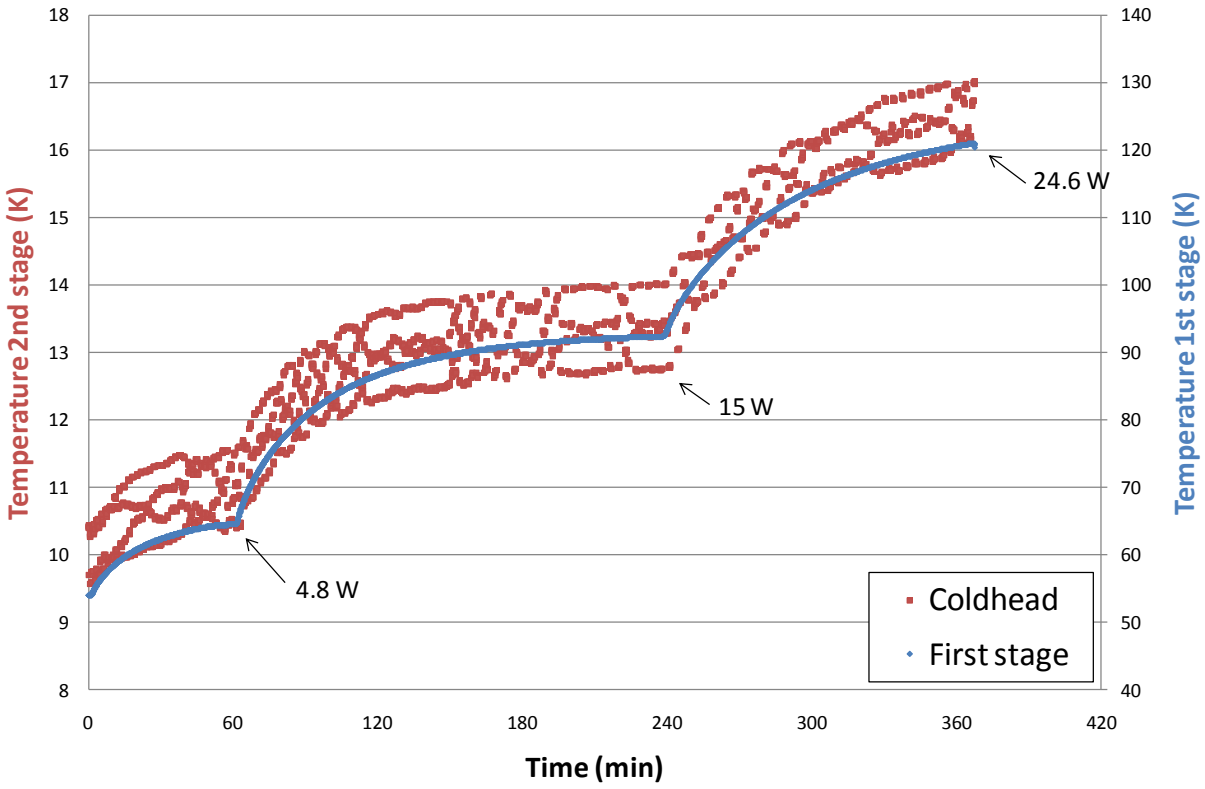

Figure 14: Coldhead and first stage temperature as a function of heating duration for three different power levels of first-stage heating.

Figure 15 shows the temperature/heating power relationship for first-stage heating. Compared to the coldhead, the first stage is able to sink significantly more power (> 25 W) without raising the coldhead temperature to temperatures higher than 20 K. The coldhead temperature as a function of first stage heating power from [11] is slightly higher than the values measured in this work, and the reported first-stage temperature values remain 12-18 K below the values measured here.

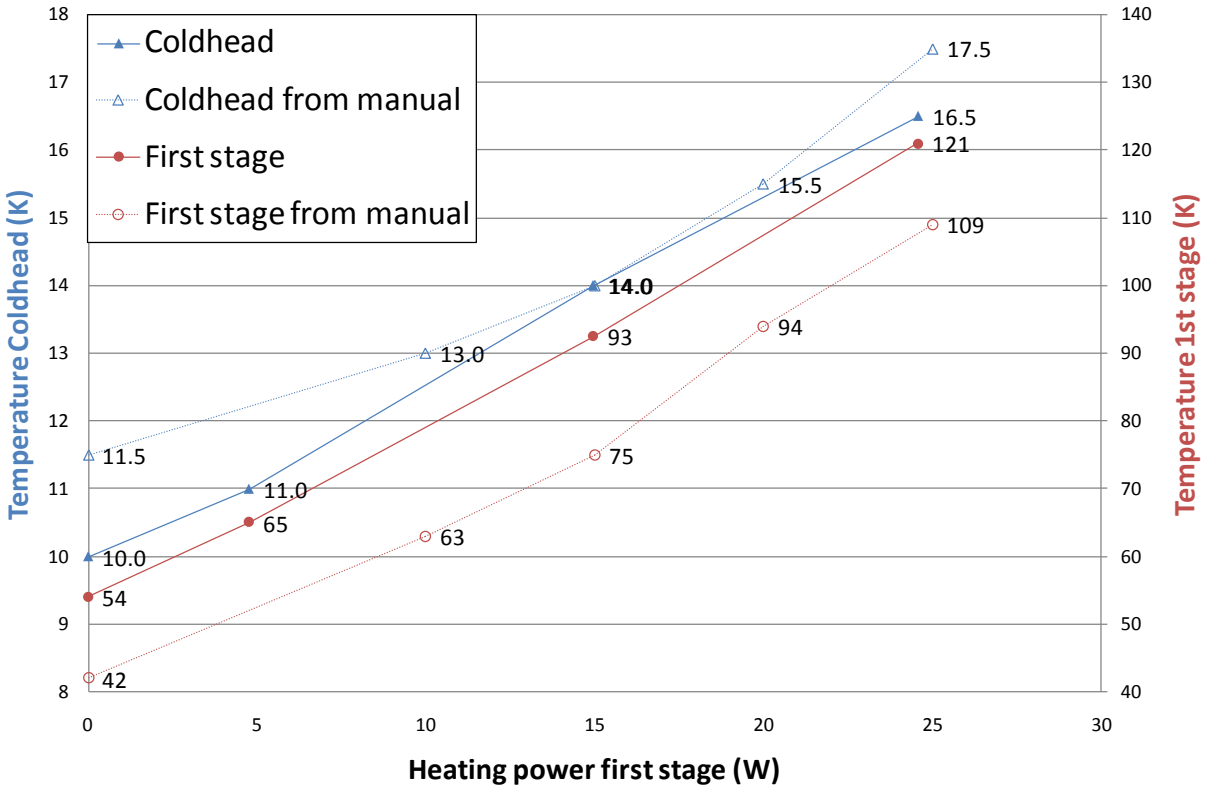

Figure 15: Comparison of the temperatures as a function of power in first-stage heater measured in this work and reported in [11].

Figure 16 shows the temperature that is achieved at the first stage and at the coldhead as a function of the power that is input into the coldhead heater. To remain below 20 K a maximum heat load of 5.5 W into the coldhead is permissible.

For comparison the performance data from the cryocooler manual [11] is plotted as well. At the same heating power the coldhead temperatures reported in [11] are about 2 K higher, while the first stage temperatures are about 10 K lower than those measured in this work. The exact conditions of the performance measurement done by CTI-Cryogenics are not specified in [11].

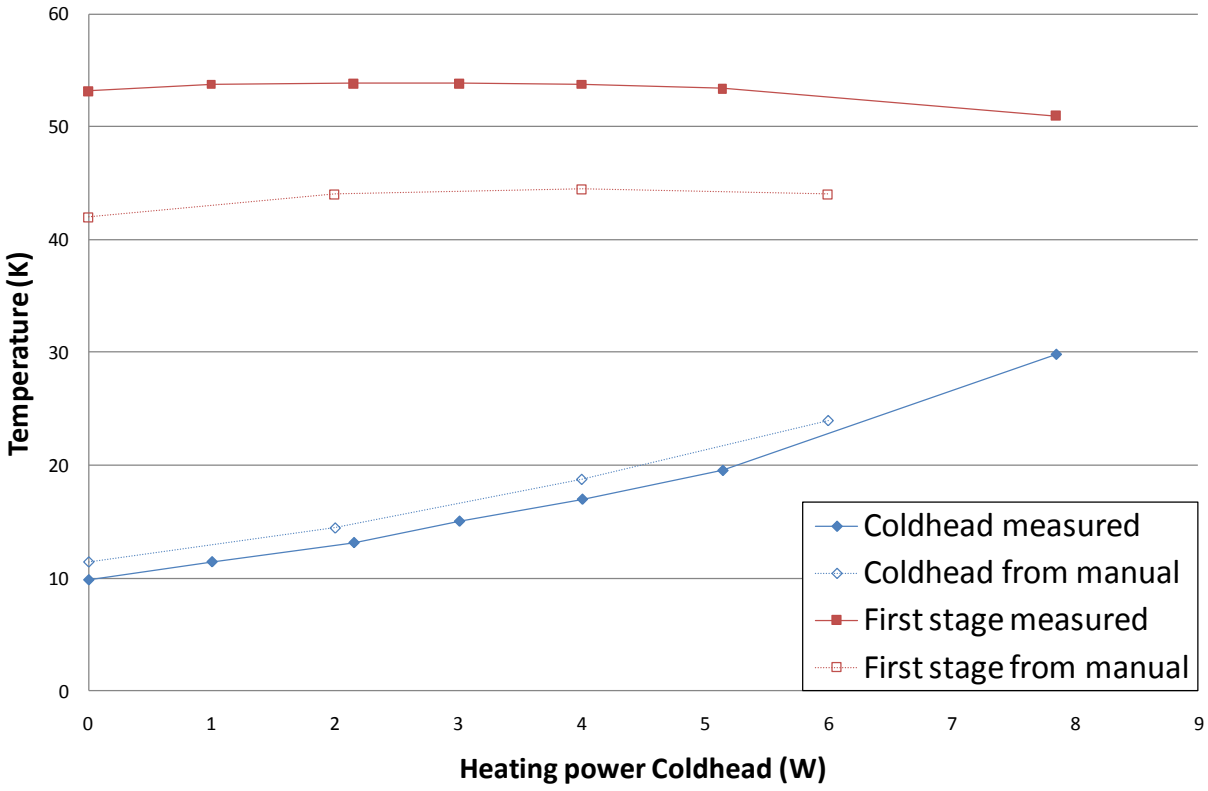

Figure 16: Comparison of the coldhead and first-stage temperature as a function of power in coldhead heater measured in this work and reported in [11].

When graphing the temperatures achieved with the final current lead design into the performance map supplied by CTI-Cryogenics (represented by the grey spot in the middle of Figure 17), the heat load by conduction through the current leads can be estimated as 14 W into first stage and 5 W into the coldhead.

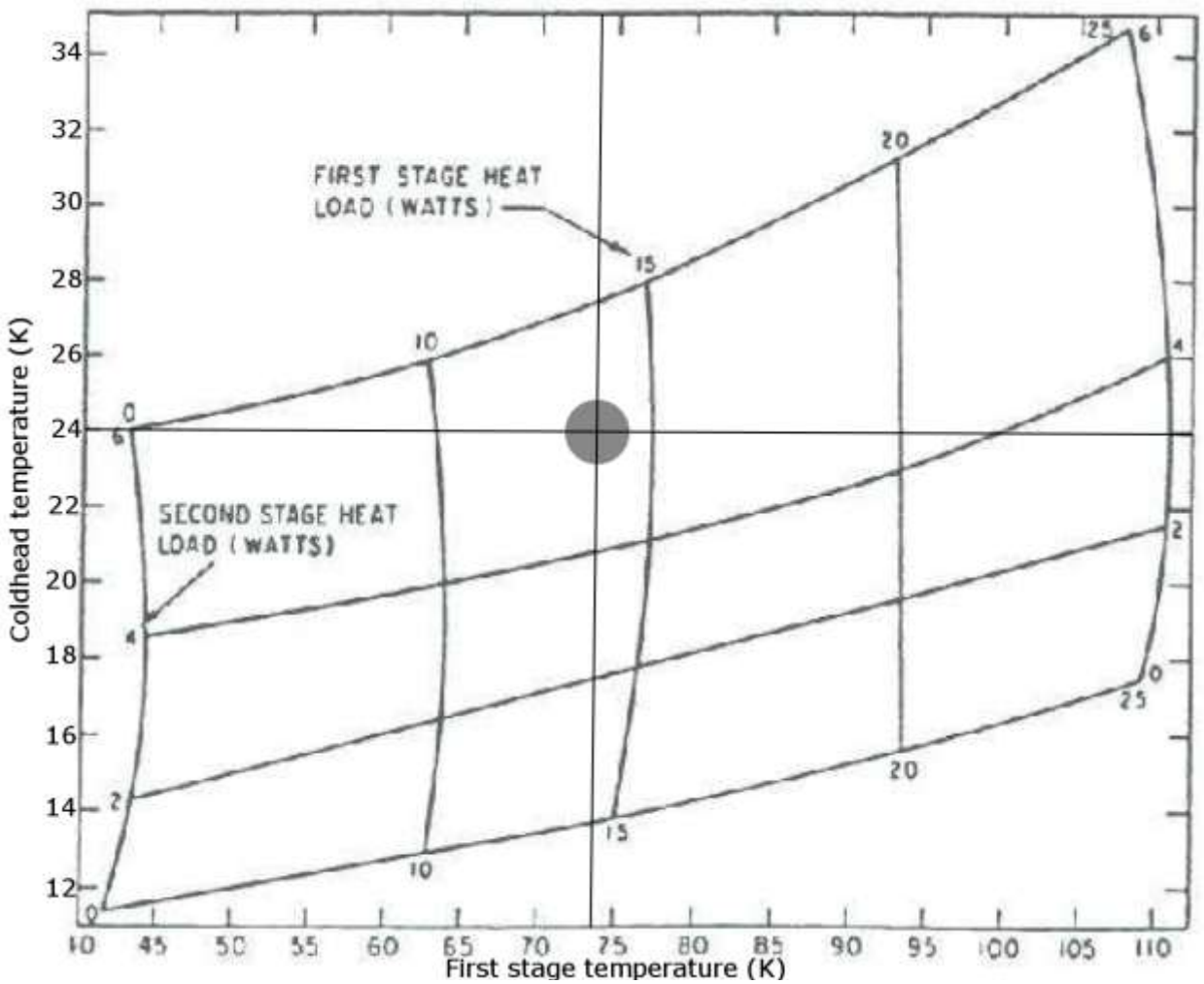

Figure 17: Performance map of Cryodyne Model 350C two-stage refrigeration system with Model 8500 compressor operated at 50 Hz. Grid-lines at 74 K and 24 K represent the final current lead design during lap-splice measurements. Original map taken from [11]. Modified by R. Lutum.

The minimum temperatures that were achieved with the cryocooler setup with and without sample and current leads are represented in the cool-down curves shown in Figure 18. The measurements without current leads show that a final temperature of around 10 K can be achieved regardless of the absence or the type of a sample, but obviously the cool-down time increases with sample mass. The time required to reach the minimum temperature is between 2.5 h and 4.5 h.

Due to the additional heat load on the cryogenic system the achievable temperature rises to approximately 17 K and 23 K when the samples are instrumented with the current leads as described in 2.2.6 with 3.1 mm² and 6.3 mm² cross section, respectively. The reason for the longer

cool-down time in the case of the butt-splice sample as compared to the more massive lap-splice sample is not understood.

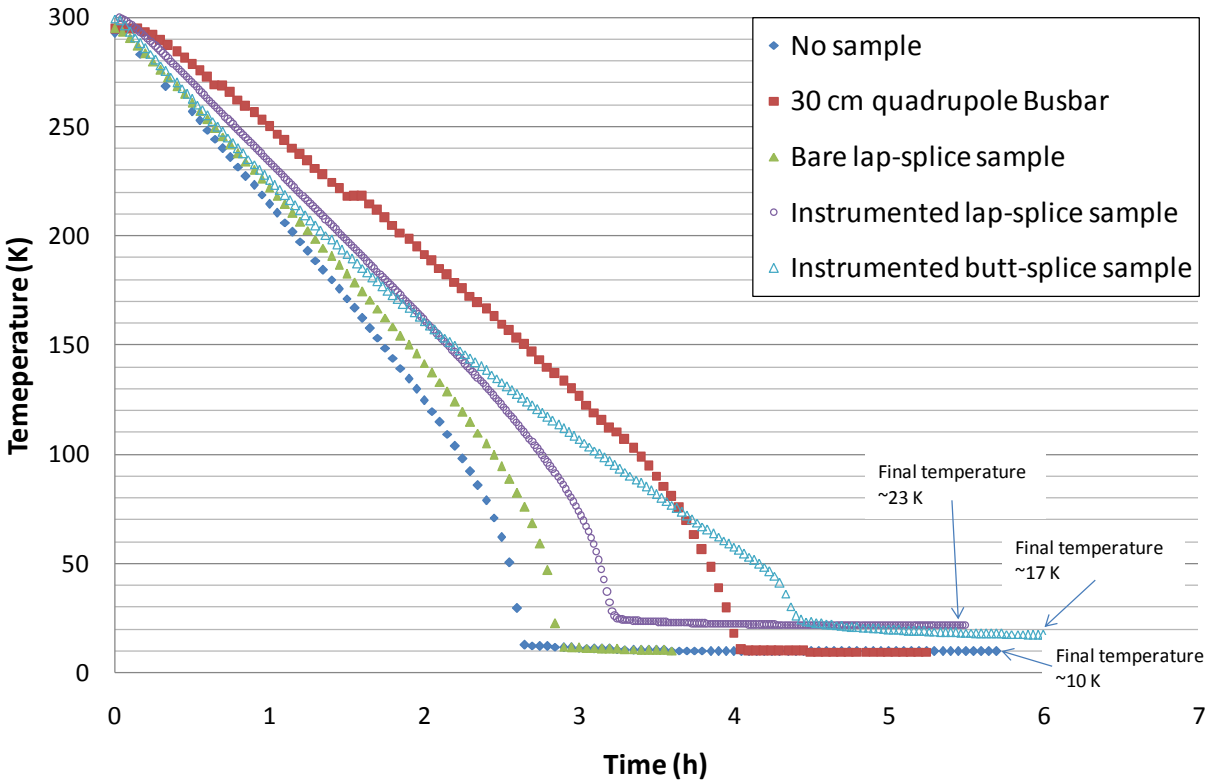

Figure 18: Sample holder cool-down curves without sample and with different sample types and instrumentation.

Table 1 shows the lowest sample temperatures that could be achieved for various experimental configurations.

Table 1: Achievable temperatures and estimated heat loads for different experimental configurations of the cryocooler setup.

Instrumentation status	**Minimum sample temperature**	**Corresponding heat load into Coldhead, estimated from results of heating experiments**
Heat shield mounted, no measurement wires, no current leads	< 10 K	Definition of 0 W additional heat load
Voltage measurement wires, 0.1 mm diameter, lacquer insulation, thermalised	< 10 K	No measureable temperature increase
0.5 mm Voltage measurement wires not thermalised	17 K	4 W
Heat shield removed	31 K	8 W
Heat shield removed, 6.3 mm^2 current leads connected to sample, not thermalised	60 K	13.5 W 5.5 W from current leads 8 W result from missing heat shield
Heat shield attached, 6.3 mm^2 current leads, not thermalised	52 K	12 W
Heat shield attached, 6.3 mm^2 current leads, thermalised by taping to heat-shield support	21 K	5.5 W
Heat shield attached, first-stage thermalisation complete, 12.6 mm^2 current leads, improvisational thermalisation on sample holder	24 K	74 K on first stage, 14 W of first stage and 5 W on second stage, estimated from performance map

2.4. Resistance measurement

2.4.1. Current regulation

The current for the resistance measurement is supplied by a Delta Electronics SM 30-200 Power Supply, capable of delivering 0-200 A in a voltage range of 0-30 V. For a more accurate current setting than possible via the three-digit current display on the front-panel, a Thurlby Thandar TSX1820P power supply is connected to the analogue current program input. The SM 30-200 is set to "remote constant current" operation, and a voltage of 0-5 V is supplied to the current program input resulting in a proportional current output of 0-200 A.

2.4.2. Voltage measurement

The voltage drop between the voltage taps is measured with an HP 3458A DMM on the R_trans/R_2 taps, and with a Keithley DMM2001 on the R_6/R_5 taps (see Figure 21 and Figure 23 (a) for a definition). The voltage taps are connected to the Jaeger-connectors with insulated single strand wire of about 0.1 mm conductor diameter.

2.4.3. Data acquisition and measurement process

When the sample is cooled down to its minimum temperature of typically 23 K, a LabView recording is started with 750 ms sample time (which results in a spacing of the sampled data points of about 800 ms in time). The power supply is programmed via the analogue current program input to 20/150 A and the current is switched on. On the LabView window the recorded data points can be observed, and once the voltage readings have reached a stable level, the current remains turned on for a period of four to eight samples. The power supply output is then switched off, and the sample is allowed to cool-down to its initial temperature (requiring around 90 s for a lap-splice sample around 23 K). In the meantime the current leads connecting the power supply to the current feedthrough are switched in their polarity. The measurement cycle is then repeated with a current of opposite sign.

For resistance measurements below 35 K, the sample temperature is regulated by varying the heater power. When a stable temperature is reached, the power to the heater is switched off. A new recording is started, and once the sample-temperature starts dropping again, the measurement is executed as described above. This way the sample does not heat up much due to resistive heating of the current leads, since the energy introduced can be dissipated right away.

Above 35 K achieving a stable temperature via heating is not feasible anymore, as the supplied heat energy causes a runaway of the temperature, or it takes too long until a stable temperature is reached. Therefore the heating strategy is changed. The heater is now supplied with maximum power (~65 W) until about five to seven K before target temperature. The temperature then rises another five to seven K without heat-energy being supplied into the system. Around the turnover of the temperature change (conversion from sample temperature rising to dropping again) a period with very small temperature change is achieved. The measurements with 20/150 A and -20/-150 A can be executed within a small temperature window and with little time between them. This is possible, because the effect of resistive heating is partially cancelled out by the cooling power of the refrigeration system.

Figure 19 shows the LabView user interface used for data acquisition during the measurement process. The upper graph shows the two voltage signals of U_trans/U_2 (white) and U_6/U_5 (turquoise) in Volt. The graph in the middle shows the temperatures of the busbar (red) and of the shunt (turquoise) or respectively the top and lower part of the butt-splice sample in Kelvin. The lowest graph represents the pressure inside of the cryostat in millibar.

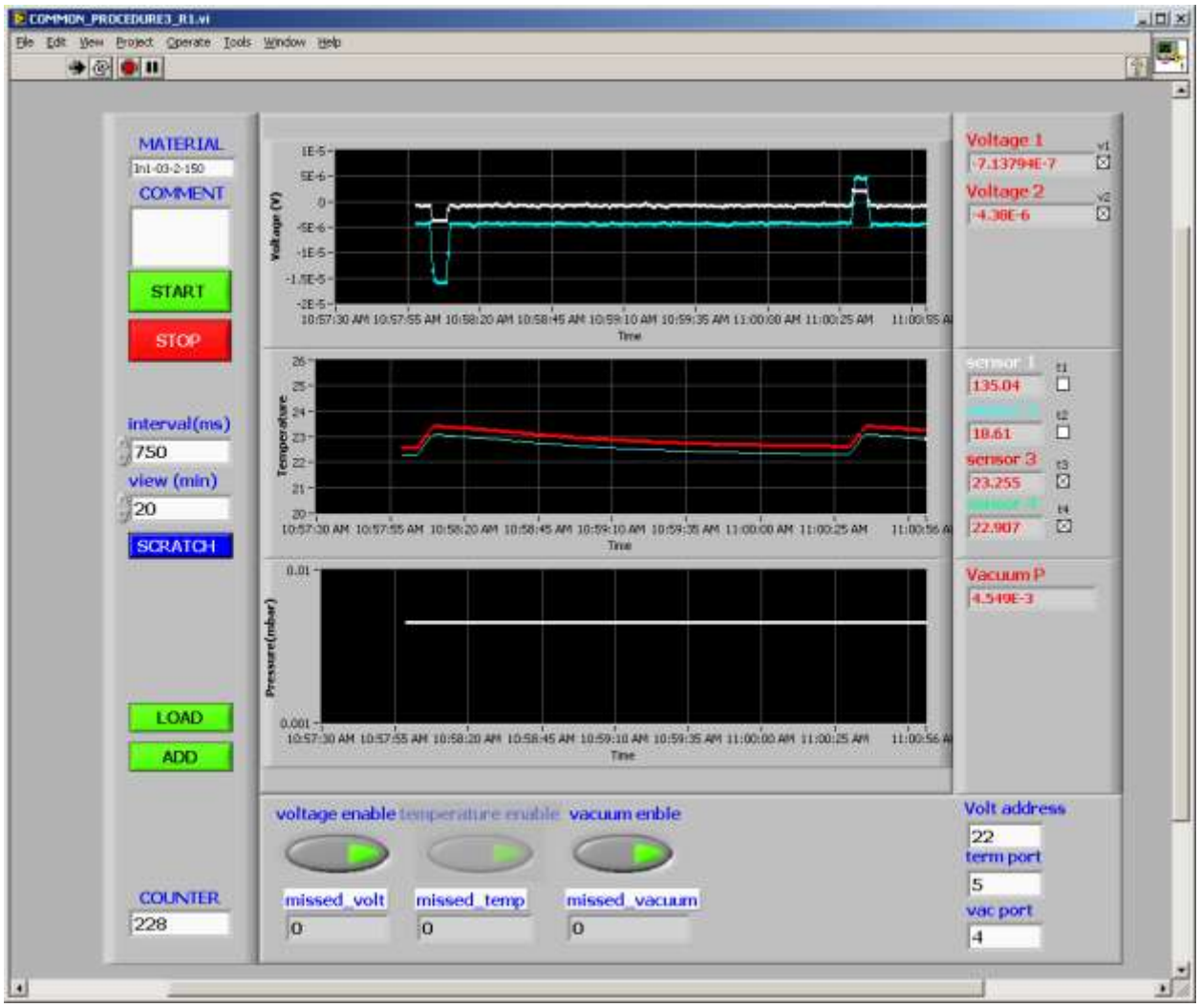

Figure 19: LabView user interface for data acquisition; measurement of Sn77.2In20Ag2.8_1 around 22 K in progress.

2.5. The solder samples

Figure 20 summarizes the electrical resistivity values for different solder alloys as a function of temperature. The solder alloys selected for this experiment are Sn96Ag4, Sn60Pb40 and Sn77.2In20Ag2.8. Sn96Ag4 is the solder used for the inductive soldering of the LHC main interconnection splices. Sn60Pb40 is foreseen for the soldering of the Cu shunts for the main interconnection splice consolidation. In order to investigate the influence of the resistivity of the solder on the overall splice resistance, the Sn77.2In20Ag2.8 solder with a comparatively high 4.2 K resistivity of 67 nΩm was tested as well [13].

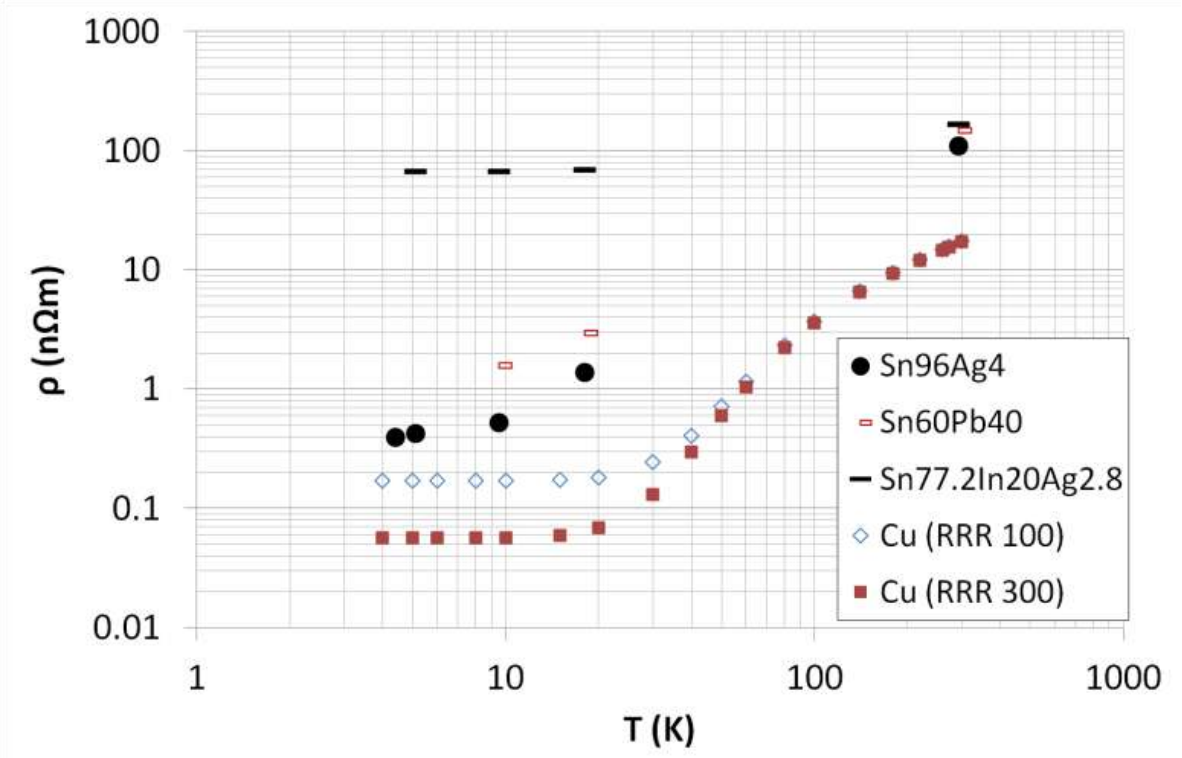

Figure 20: Electrical resistivity ρ as a function of the temperature T of selected solder alloys. The solders selected for this study are Sn60Pb40, Sn96Ag4 and Sn77.2In20Ag2.8. For comparison the resistivities of Cu with a RRR of 100 and 300 are shown as well. Courtesy S. Heck.

2.5.1. Sample type 1: LHC busbar-shunt lap splices

The lap-splice samples consist of a 100 mm-long LHC Quadrupole busbar [4] and a 15×80×3 mm^3 copper strip (shunt), soldered together with a solder contact cross section of 15×15 mm^2. The Cu shunts were annealed for 2 hours at 400 °C in order to increase the RRR of the initially cold worked Cu sheets. The RRR of the Cu shunt is >400, and the RRR of the LHC busbar stabilizer is >200 [14].

A photograph of an instrumented sample is shown in Figure 21 (a). At each end of the sample an M5-thread was tapped to mount the current leads. On the busbar there is a ø6 mm through-hole to mount the sample on the cryocooler sample holder. Two M3-threads were tapped to allow mounting of temperature probes.

For voltage measurements four strips of copper (5×40×0.5 mm^3) were bonded to the sample via electron-beam welding. Two of these are attached to the shunt (one 30 mm from the shunt-end at the solder connection, one in the middle of the connection). The remaining two are attached to the busbar (one 30 mm from the shunt-end at the solder connection, the other one opposite to the one on the shunt at the connection). Figure 21 (a) shows the front and the back of a lap-splice sample with synthetically insulated wires manually soldered to the voltage taps. These were used for RT and liquid Nitrogen measurements. For the measurements in the cryocooler, the voltage taps were shortened to about 15 mm length in order to fit under the heat-shield. Figure 21 (b) shows an electrical equivalent circuit defining the naming scheme used in this document.

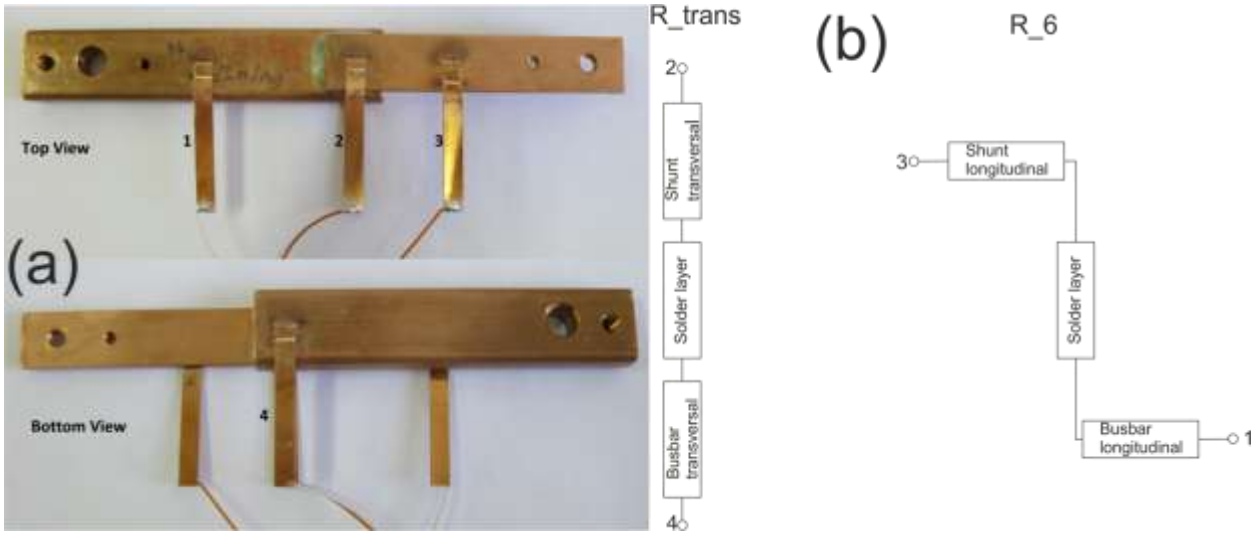

Figure 21: (a) Busbar to shunt solder connection with electron-beam welded potential taps, threads for current lead and temperature probe connection. (b) Equivalent circuit of R_6 and R_trans.

2.5.2. Sample type 2: Butt splices

The butt-splice samples consist of two equal copper pieces that are soldered together with Sn60PB40 solder and different solder fluxes (so called MOB and Kester). The cross section in the solder area is approximately 4×4 mm^2, and the solder thickness is in the range of 150-200 µm. Six samples were tested, one of which is a pure copper sample to use as a reference. The samples K1 (Kester1), M1 (MOB1) and MX (MOBX) are so-called "machined" samples. Into a flat strip of copper a cut-out of approximately 150 µm was made (see Figure 22 (a)). The solder-alloy was then applied into that cut-out and after soldering the excess-material was removed from the centre cross-section. The samples then had the shape as specified in Figure 22 (b). The other samples, K3 (Kester3) and K4 (Kester4), consist of two Cu-profiles machined to the final shape, which were then joined via soldering as a last step in manufacturing, to compare the achievable tolerances to those of the machined samples.

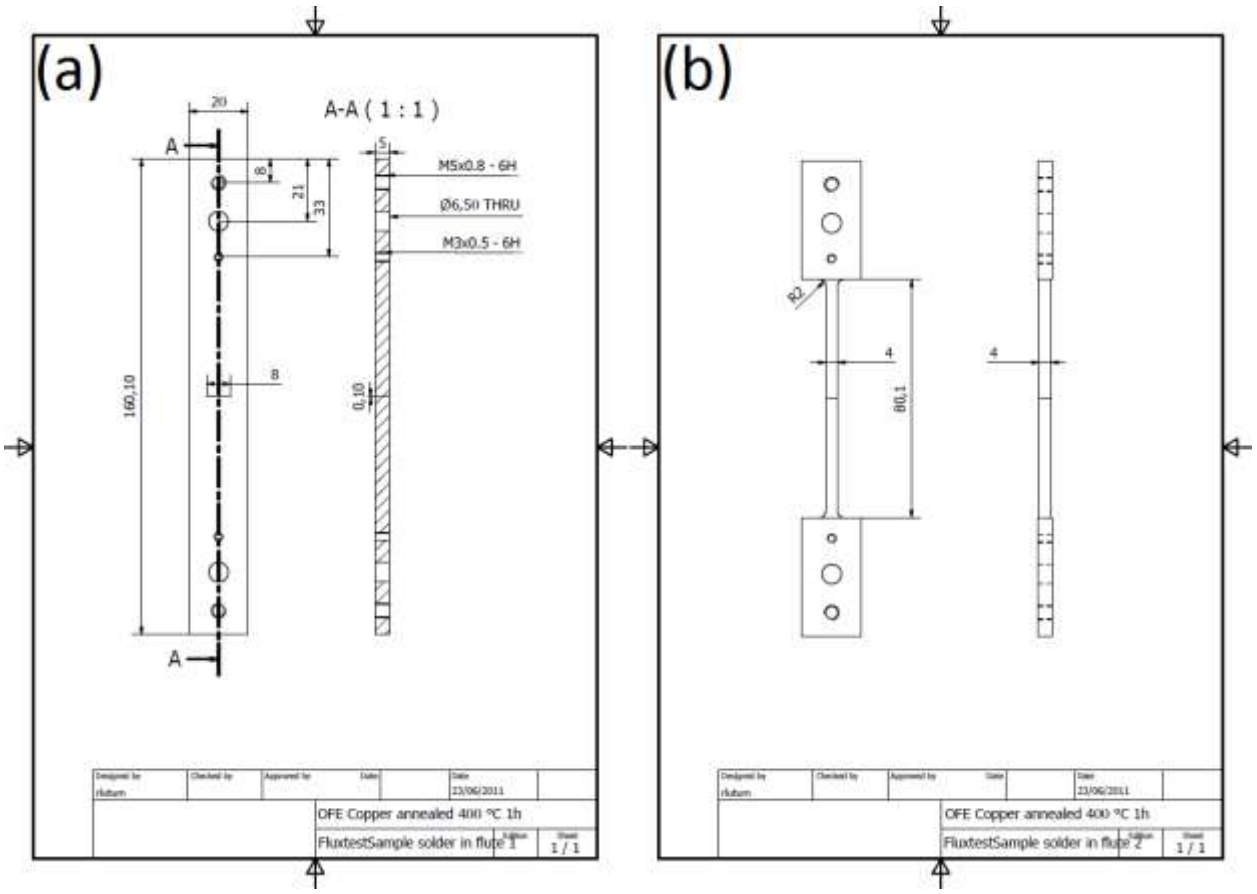

Figure 22: Technical drawings for manufacture of butt-splice samples. (a) Before soldering and milling. (b) After soldering and milling.

Figure 23 (a) shows sample M1 and the pure copper sample (Cu) with manually soldered voltage taps. The distance between the voltage taps is 20 mm or 50 mm (so called R_2 and R_5 respectively). Also visible is the polyimide tape used to electrically insulate the samples against the sample holder of the cryocooler. Figure 23 (b) shows a detail of the solder layer of sample M1.

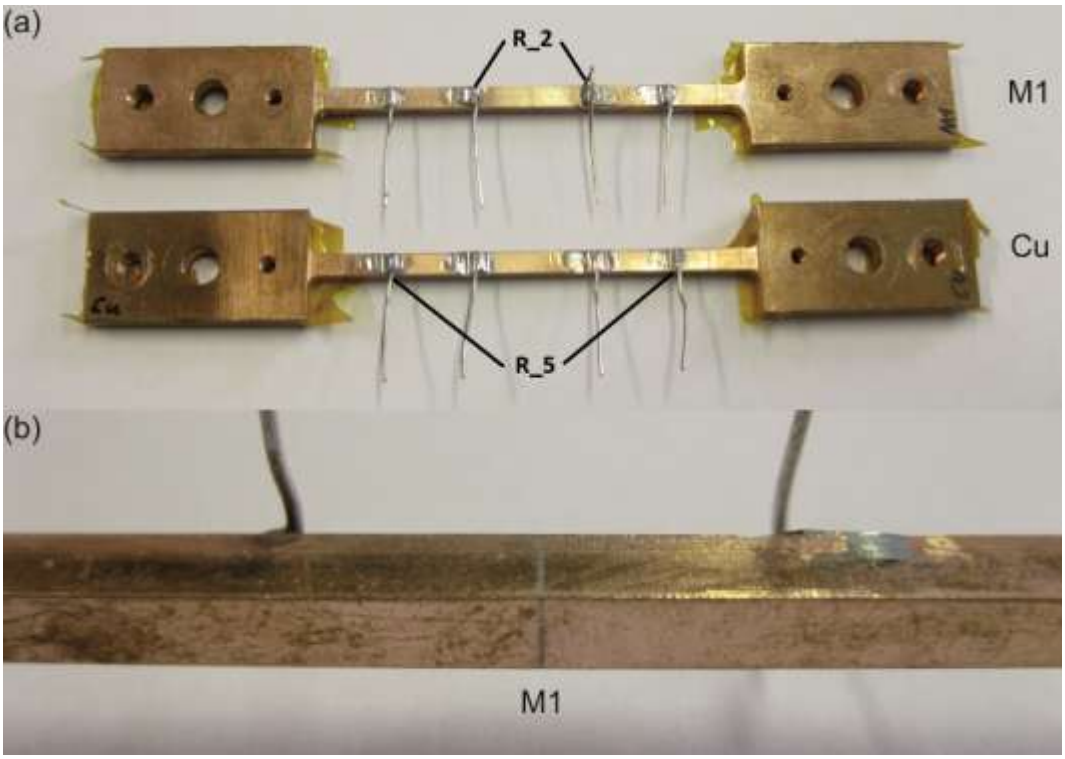

Figure 23: (a) Instrumented butt-splice samples M1 (machined MOB sample) and Cu (machined pure copper). (b) Detail view of M1 solder connection.

Figure 24 shows samples K1, K3, K4 and MX after they were fractured during a tensile test. The lower part of Figure 24 shows the fractured solder contact cross sections.

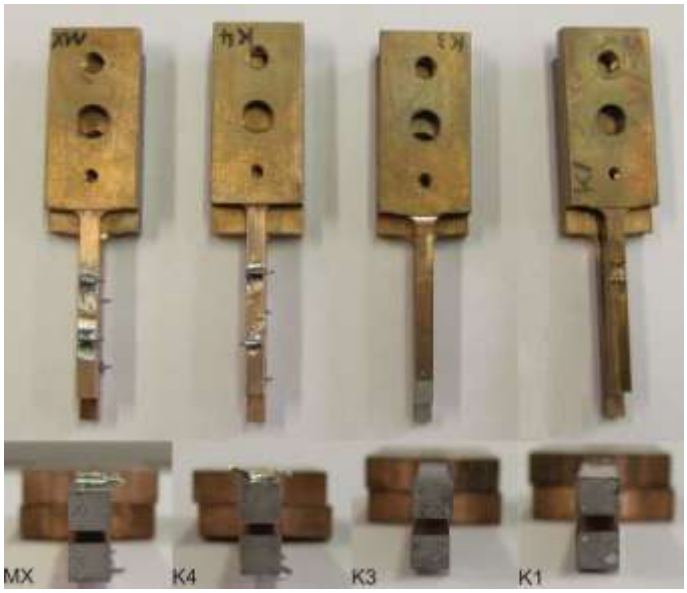

Figure 24: Butt-splice samples K1, K3, K4 and MX, with details of the fractured solder connections (due to tensile strength measurements,).

3. Results

The resistance and resistance ratio results in the following section are all graphed on log-log plots in order to visualise the resistance variations over more than two orders of magnitude.

3.1. Electrical resistance of lap splices as a function of temperature

Figure 25 shows R_trans resistance values of all measured lap splices as a function of temperature. At 23 K the R_trans resistances of Sn96Ag4 and Sn60Pb40 splices are 5.5±1.0 nΩ and 6.1±2.4 nΩ, respectively. The R_trans value of splices soldered with the high resistivity solder Sn77.2In20Ag2.8 is about 3 times higher (16.6±2.6 nΩ).

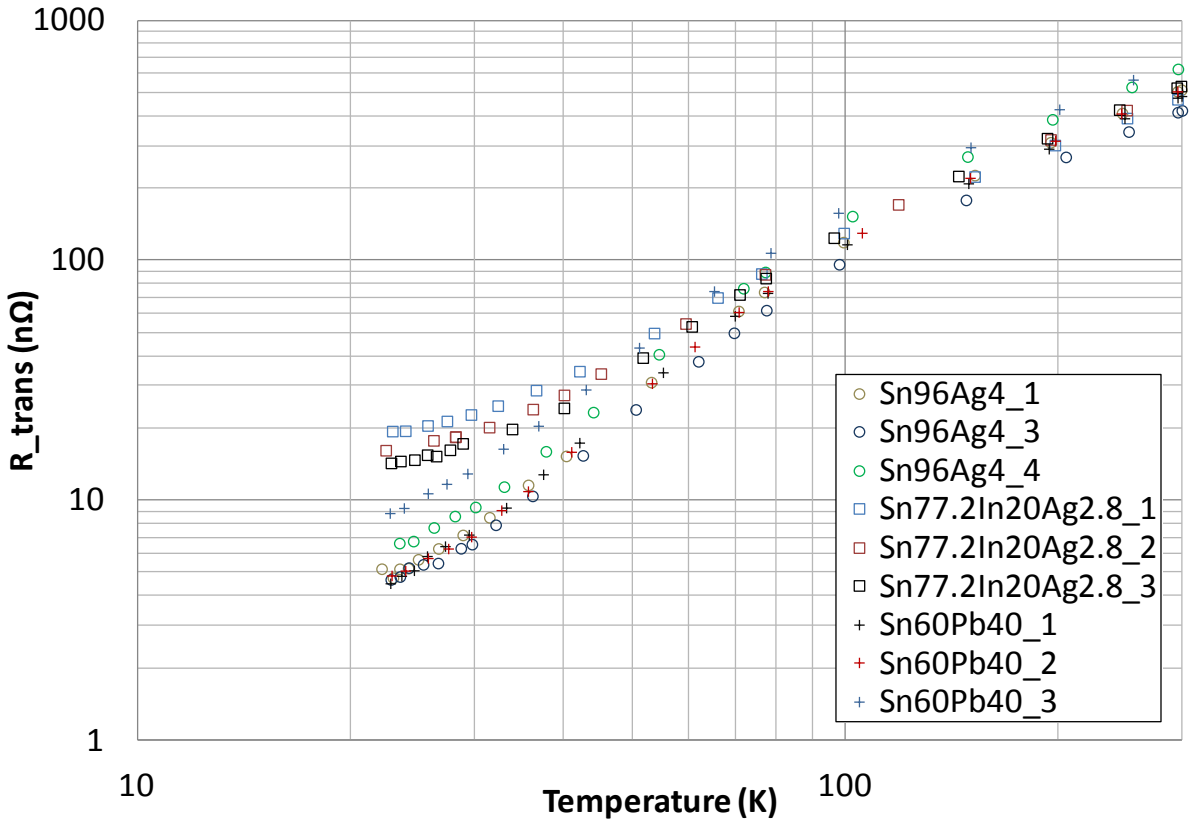

Figure 25: R_trans resistance as a function of the temperature of splices produced with Sn96Ag4, Sn60Pb40 and Sn77.2In20Ag2.8.

The corresponding resistance ratios are presented in Figure 26. For comparison the resistance ratio curves of pure copper with a RRR of 20, 50 and of 100 are shown as well. Below 100 K the data points deviate strongly from the pure copper curves, indicating a strong influence of the solder bulk resistance on the overall R_trans. At 23 K the resistance ratio of Sn77.2Ag20In2.8 soldered splices is roughly 3 times lower than that of Sn96Ag and Sn60Pb40 soldered splices.

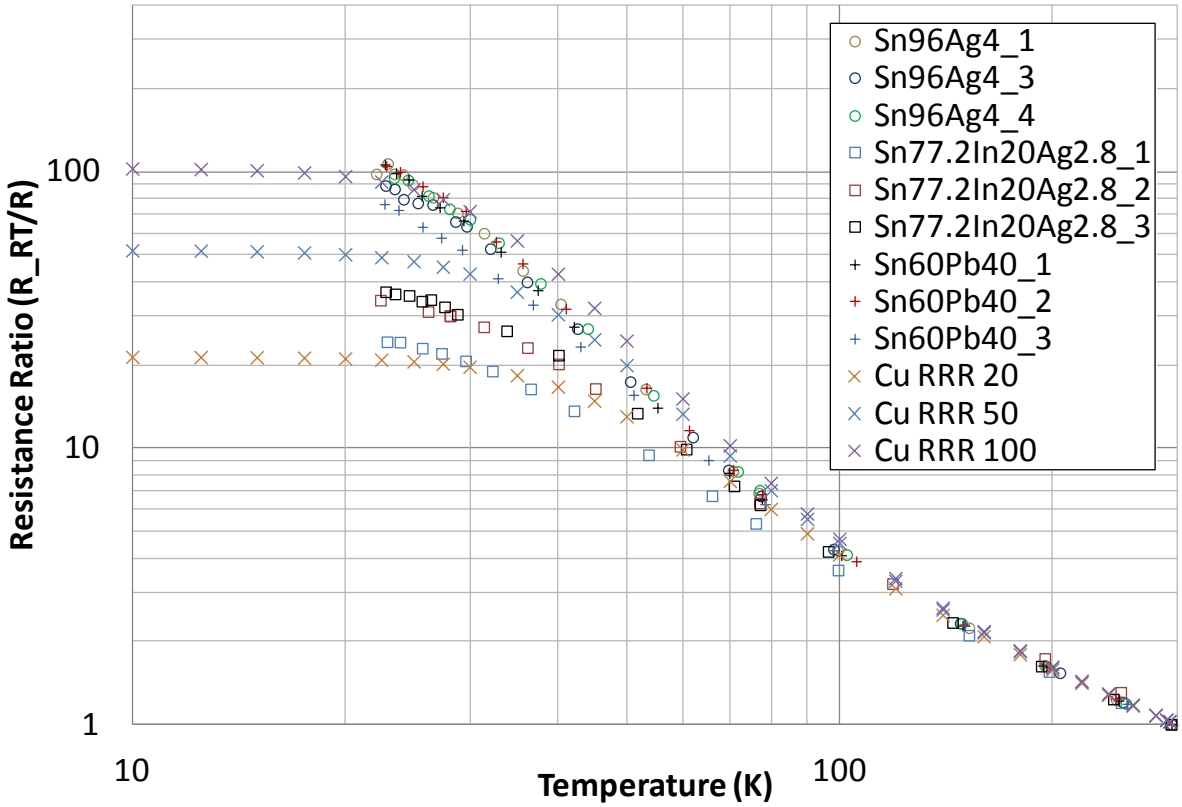

Figure 26: R_trans resistance ratio as a function of the temperature of splices produced with Sn96Ag4, Sn60Pb40 and Sn77.2In20Ag2.8. For comparison the RR of Cu with a RRR of 20, 50 and 100 is shown as well.

The R_6 resistance ratio values of all measured lap splices as a function of temperature are summarised in Figure 27. Resistance ratio curves of pure copper with a RRR of 200 and of 400 are shown for comparison. R_6 is only slightly influenced by the solder layer resistance (at 23 K: $R\_6_{Sn96Ag4}$ = 49.6±5.6 nΩ, $R\_6_{Sn60Pb40}$ = 49.5±6.4 nΩ, $R\_6_{Sn77.2In20Ag2.8}$ = 61.4±6.4 nΩ). The R_6 ratios of Sn96Ag4 and Sn60Pb40 soldered splices can be fitted approximately with resistance ratios of Cu with a RRR between 300 and 400. The R_6 ratio of splices soldered with Sn77.2In20Ag2.8 approximately follows the resistance ratio of Cu with a RRR between 200 and 300.

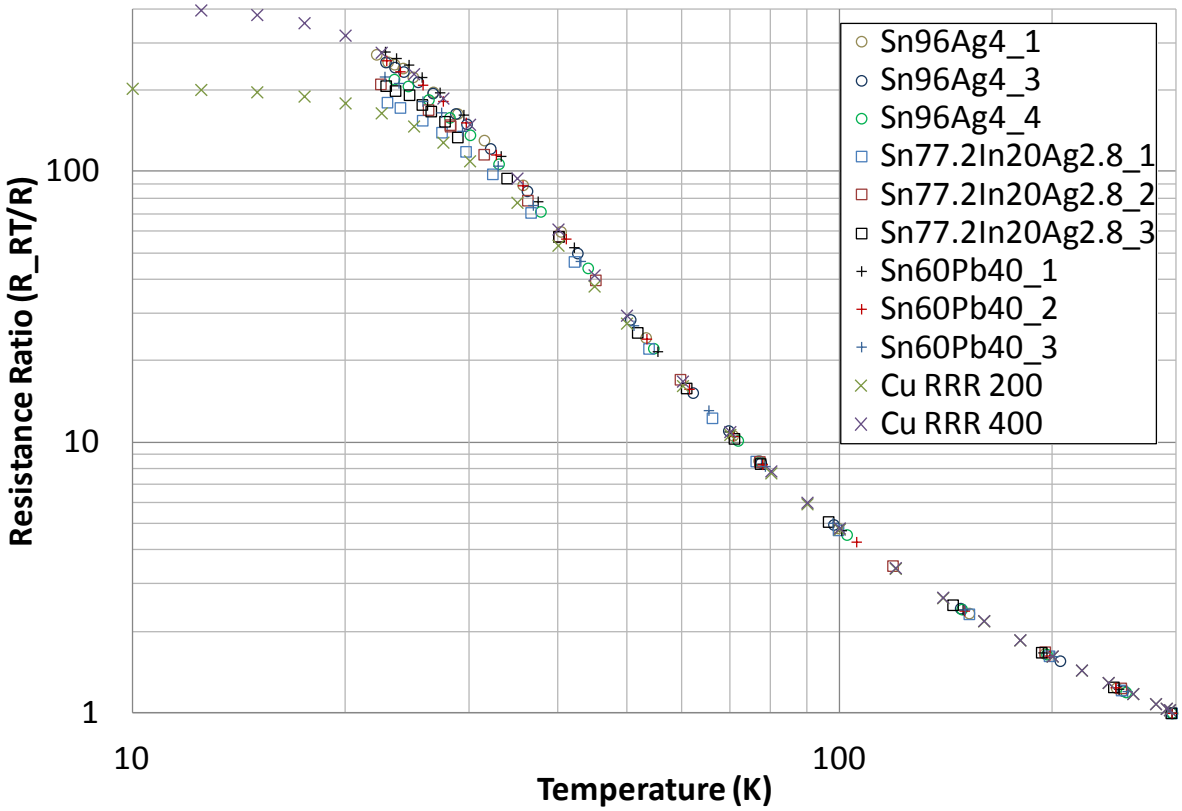

Figure 27: R_6 resistance ratio (RR) as a function of the temperature of splices produced with Sn96Ag4, Sn60Pb40 and Sn77.2In20Ag2.8. For comparison the RR of Cu with a RRR of 200 and 400 is shown as well.

The resistance values of the lap splices measured at RT and at minimum temperature in the cryocooler setup are summarised in Table 2.

Table 2: R_6 and R_trans resistances of the 9 lap splices measured at minimum and at RT.

Sample	R_trans (nΩ)	R_6 (μΩ)	Temperature (K)	R_trans (nΩ)	R_6 (μΩ)	Temperature (K)
Sn77.2In20Ag2.8_1	19.41	0.0685	22.9	469.3	12.37	295.0
Sn77.2In20Ag2.8_2	16.15	0.0596	22.4	552.0	12.57	295.0
Sn77.2In20Ag2.8_3	14.30	0.0562	22.8	524.3	11.68	294.3
Sn96Ag4_1	5.18	0.0451	22.1	506.3	12.25	294.9
Sn96Ag4_3	4.67	0.0478	22.8	414.4	12.16	295.2
Sn96Ag4_4	6.62	0.0559	23.5	627.9	12.29	295.4
Sn60Pb40_1	4.50	0.0450	22.8	476.3	12.52	295.1
Sn60Pb40_2	4.85	0.0467	22.9	506.4	12.05	294.9
Sn60Pb40_3	8.83	0.0569	22.7	672.2	12.79	295.0

3.2. Electrical resistance of butt splices as a function of temperature

Figure 28 shows the electrical resistance values of the butt-splice samples MOB1, MOBX and Kester1, together with the Cu reference sample as a function of temperature. At RT the R_5 resistance of MOB1, MOBX and Kester1 is identical within the experimental error (average R_5 value for MOB1, MOBX and Kester 1 is 58.7±1.1 μΩ). The R_2 values of MOB1 and MOBX are nearly identical as well (26.7 μΩ and 26.6 μΩ, respectively). The R_5 and R_2 values of 53.5 μΩ and 22.5 μΩ measured for the Cu reference sample are significantly lower than those of the soldered samples. Below 100 K the resistance curves of the soldered samples begin to drop slower than the ones of the pure Cu sample. At 17 K the average R_5 resistance of MOB1, MOBX and Kester1 is 383±11 nΩ. The R_2 values of MOB1 and MOBX are 197 nΩ and 204 nΩ, respectively. R_5 and R_2 of the pure Cu sample are 319 nΩ and 130 nΩ, respectively.

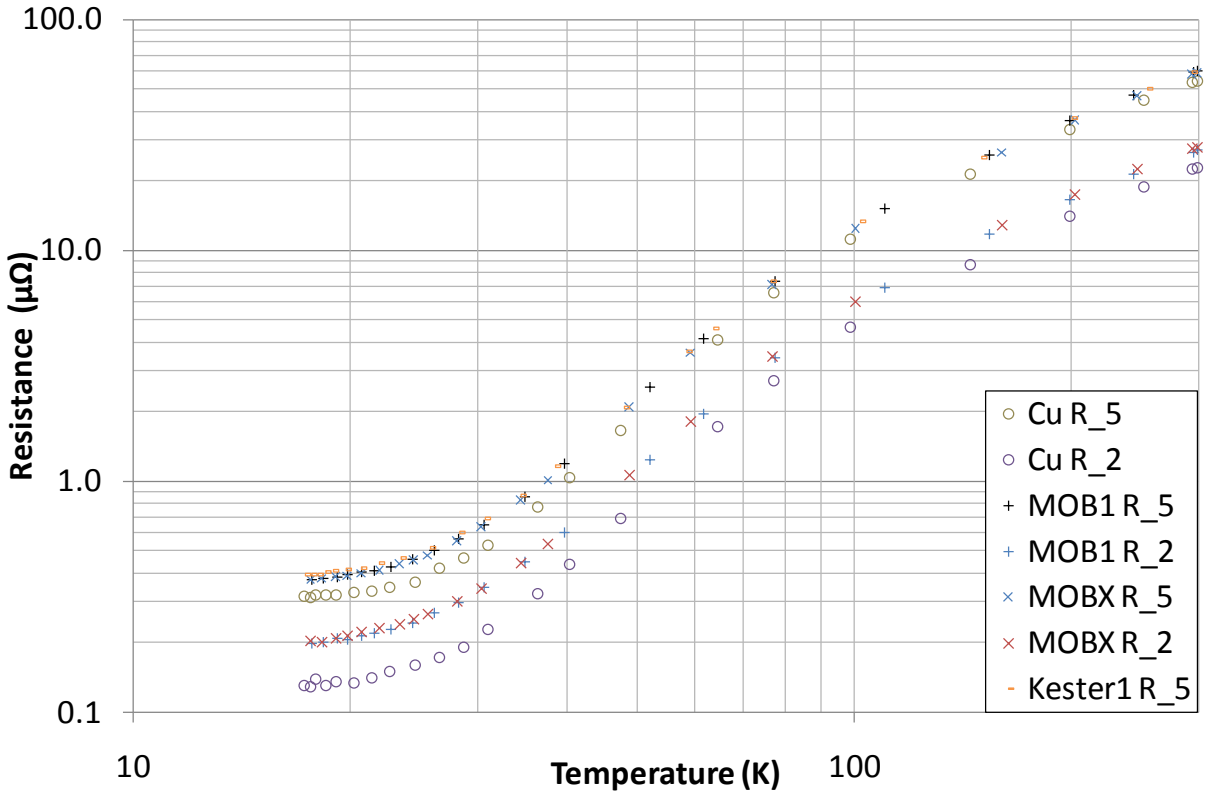

Figure 28: R_5 and R_2 resistance values of butt-splice samples soldered with Sn60Pb40 and of unsoldered Cu sample as a function of temperature.

Table 3 summarises the R_2 and R_5 resistance values of the butt splices measured at RT and at minimum temperature in the cryocooler. There is no significant difference in the resistance of the samples soldered with different flux.

Table 3: R_2 and R_5 resistances of the four butt splices measured at minimum and at RT.

Sample	R_2 (μΩ)	R_5 (μΩ)	Temperature (K)	R_2 (μΩ)	R_5 (μΩ)	Temperature (K)
MOB1	0.197	0.376	17.7	26.7	59.1	295.3
MOBX	0.204	0.376	17.6	27.6	57.5	295.1
Kester1	N/A	0.395	17.3	N/A	59.5	294.9
Cu	0.130	0.319	17.3	22.5	53.5	294.5

Figure 29 shows the R_5 and R_2 resistance ratios of the butt-splice samples as a function of temperature, and resistance ratio curves of copper with a RRR of 120 and 180. The R_2 resistance ratios of samples MOBX and MOB1 are both 135 at 17 K. The Kester1 sample was not instrumented for an R_2 measurement. The average R_5 resistance ratio of the three soldered samples is 154±3 at 17 K. The pure Cu butt-splice sample does not show a noticeable difference between the R_2 and the R_5 resistance ratio at 173 and 168, respectively, at 17 K. The RT to 17 K resistance ratio corresponds with a Cu RRR of about 180.

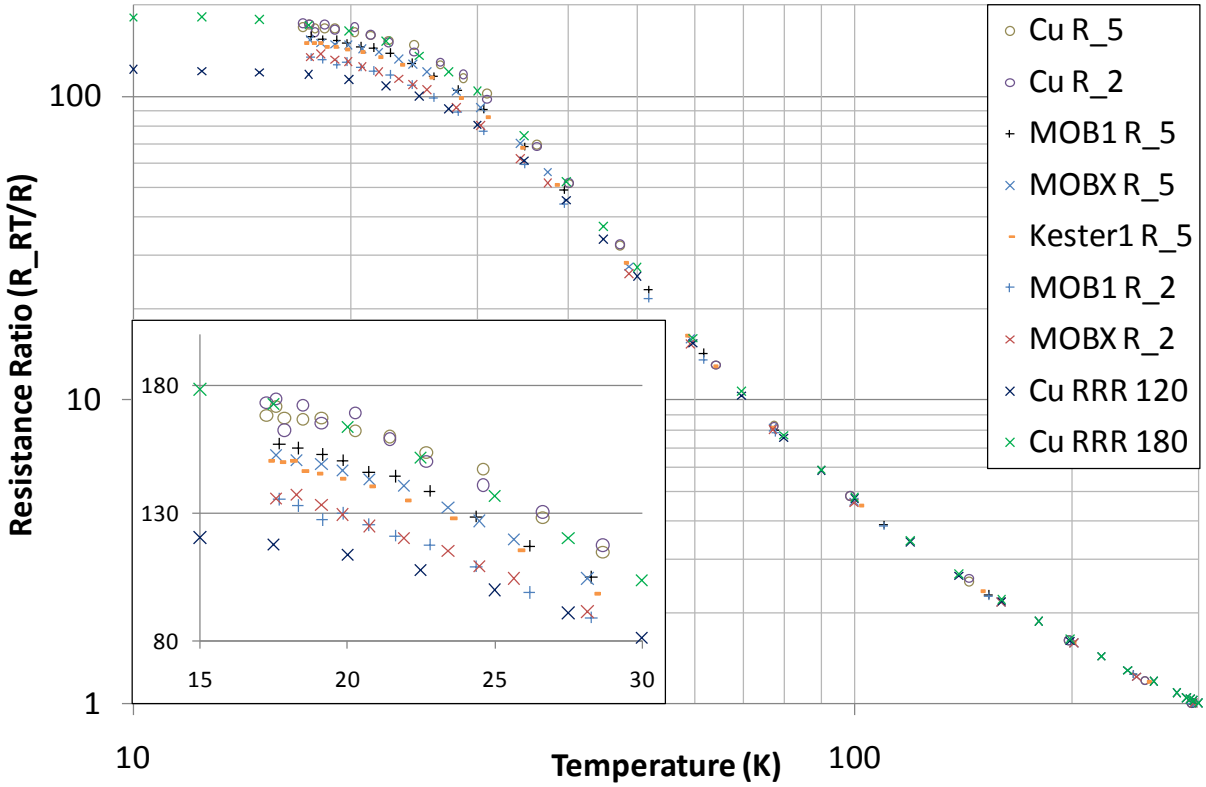

Figure 29: R_5 and R_2 resistance ratios of butt-splice samples soldered with Sn60Pb40 solder using different soldering fluxes, as a function of temperature, with detail of the 15-30 K range. Cu is an unsoldered (pure Copper) sample of same dimensions as the soldered samples. For comparison the resistance ratios of pure copper with a RRR of 120 and 180 are shown as well.

3.3. Metallographic and mechanical splice examination

3.3.1. Solder layer thickness in lap splices

The solder layer thickness was determined in metallographic cross sections prepared in the centre of four lap-splice samples. The cross-sections are shown in Figure 30. The solder thickness varies strongly across the solder layer in the approximate range of 10-220 µm for the sample Sn77.2In20Ag2.8_1, of 18-30 µm for Sn77.2In20Ag2.8_3, of 20-140 µm for Sn60Pb40_2 and of 10-150 µm for Sn96Ag4_4.

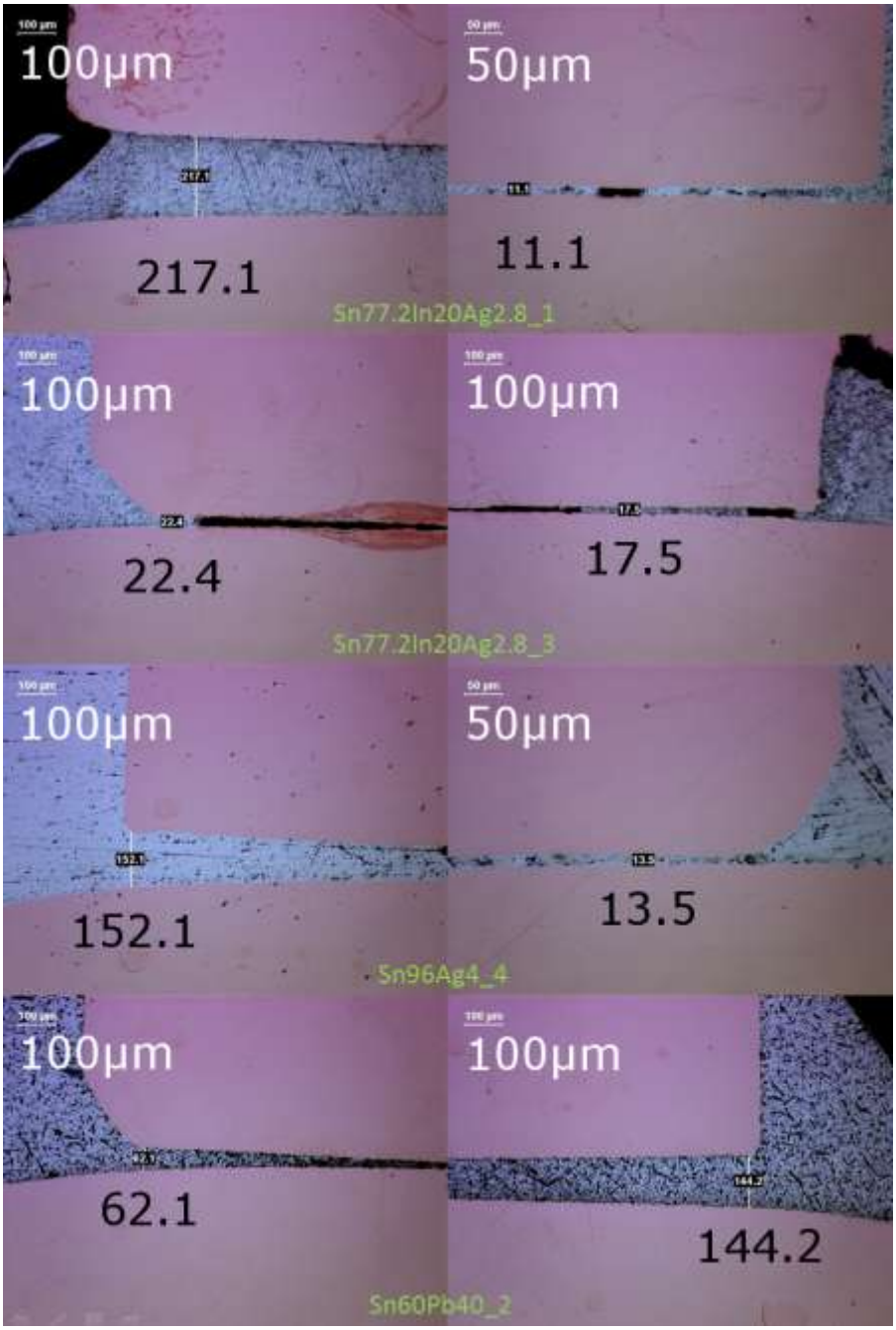

Figure 30: Metallographic cross-sections of samples Sn77.2In20Ag2.8_1, Sn77.2In20Ag2.8_3, Sn96Ag4_4 and Sn60Pb40_2.

3.3.2. Vickers hardness of the lap splices

The Vickers Hardness was measured on the shunt to busbar lap splice samples in order to estimate their RRR from the relationship between HV2.0 and RRR that had been found previously for high purity Cu with different degree of cold work [14]. The hardness of the shunt is HV2.0=52.3±5.9, corresponding to a RRR of above 300 and the busbar hardness is HV2.0=65.8±6.5, which corresponds to a RRR of about 200. There was no significant variation in Vickers hardness between the measured samples.

3.3.3. Solder layer thickness in butt splices

In the butt splices precise solder thickness measurements could be performed by digital image analysis in the optical images that have been acquired with a metallographic microscope (Olympus BX51). Figure 31 shows macroscopic images of the four sides of the solder joints of samples Kester1 and MOB1.

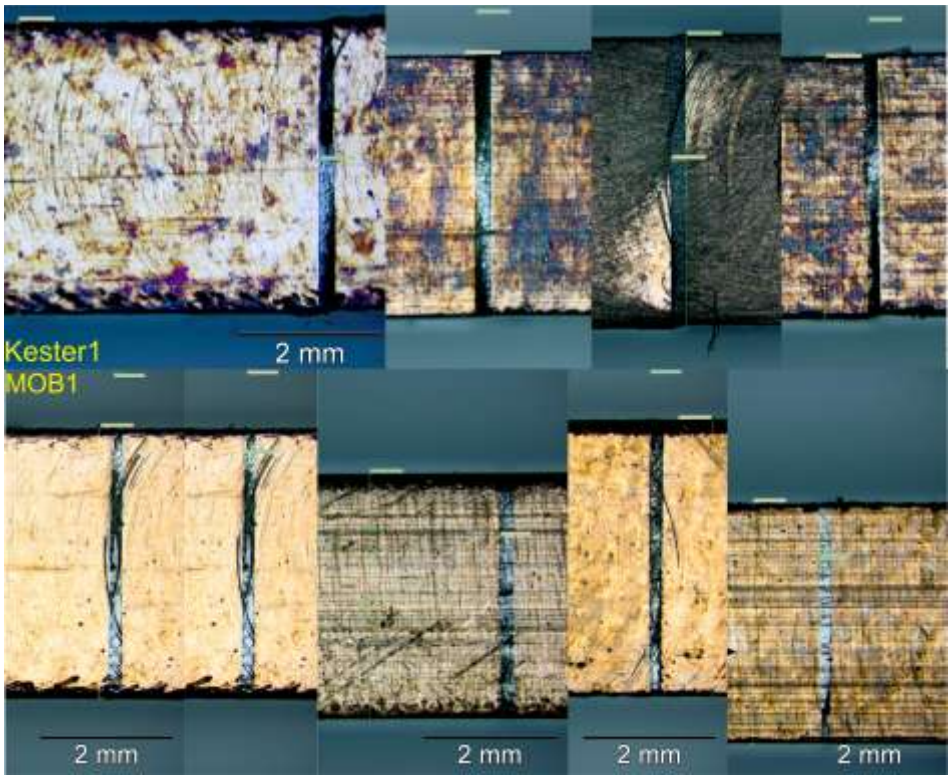

Figure 31: Microscopic images of the solder joint of Kester1 and MOB1.

The exact splice cross-sectional areas have been determined as well by digital image analysis. Unfortunately the initial sample cross section of 4×4 mm2 has been somewhat reduced during the soldering process. Table 4 summarises the measured solder cross sections and thicknesses.

Table 4: Solder layer dimensions of Kester1 and MOB1.

Position	Width (µm)	Average	Cross-section (mm²)	Solder thickness (µm)	Average
Kester1					
Top	4065	4069	14.70	206	195
Bottom	4073			191	
Left	3621	3613		206	
Right	3605			175	
MOB1					
Top	4065	4113	15.02	155	186
Bottom	4161			206	
Left	3692	3652		214	
Right	3613			167	

The bulk resistance of the solder layer at 18 K can be determined from the solder thickness, cross section and Sn60Pb resistivity of 2.98 nΩm that has been measured at 18 K [13]. The Cu R_2 and R_5 values were determined with a resistivity of 0.101 nΩm, corresponding with the RT resistivity of 17.2 nΩm [15] divided by the measured resistance ratio of 170. The Cu R_2 and Cu R_5 values are then added to the calculated solder layer resistances to obtain R_2 and R_5 of the soldered connections. Table 5 shows the results of this calculation. Good agreement is found between calculated and measured resistances for the unsoldered Cu reference sample, while the calculated resistances of the soldered connections are around 0.4-0.5 µΩ lower than the measured ones. This indicates that the joint resistance is not only influenced by the solder and Cu bulk resistance, as we take up in the discussion.

Table 5: Calculated and measured R_2 and R_5 resistance at 18 K. Calculated Sn60Pb40 solder layer resistance.

	Solder layer resistance calculated (µΩ)	R_2 measured (µΩ)	R_2 calculated (µΩ)	R_5 measured (µΩ)	R_5 calculated (µΩ)
Kester1	0.040	N/A	0.160	0.395	0.341
MOB1	0.037	0.197	0.157	0.376	0.338
Cu	N/A	0.130	0.125	0.319	0.314

3.3.4. Tensile strength of Sn60Pb40 soldered butt splices at RT

The force at fracture under nearly uniaxial loading of the butt-splice samples Kester1, Kester3, and Kester4 was measured at RT in the CERN metallography laboratory using a speed of 2 mm/min. The average force at fracture that was measured for the three samples is 794±214 N, which corresponds to a tensile stress of 79±19 MPa.

4. Discussion and Conclusion

4.1. Cryocooler setup performance

The Rial cryocooler system for thermal contraction measurements has been successfully modified and has proven to be a very practical tool for nΩ resistance measurements at varying temperature. The temperature can be regulated easily and the setup is quickly adaptable to varying sample geometries and test current requirements.

The minimum temperature that can be achieved with fully instrumented samples depends on the needed test current. 23 K and 17 K were reached with the current leads for 150 A and for 20 A, respectively. The minimum temperature that can be reached without sample instrumentation is 10 K.

The cool down time is approximately 4 hours. The time needed to exchange a sample is about 2 hours and warming up can be achieved within 3-4 hours when purging the vacuum with inert gas.

The maximum heat loads to achieve a certain temperature with the cryocooler set up estimated from the foil heater experiments are in reasonable agreement with those reported by the manufacturer.

The heat-load introduced by conduction through the 150 A current leads can be estimated to be around 14 W on the first stage and around 5 W on the coldhead. For the measurement of the butt-splices with 20 A test current, the heat loads can be reduced to estimated 8 W and 2.5 W at the first stage and coldhead, respectively.

The performance results show that the measurement system makes efficient use of the available cooling power. Further modification to the setup (lower vacuum pressure, additional heat-shielding, extensive current lead optimisation) might slightly lower the minimum temperature, but cannot be expected to yield a significant drop in temperature. Lower temperatures can be achieved with more powerful state-of-the-art refrigeration systems.

4.2. Lap splice resistance and resistance ratio

For the consolidation of the LHC main interconnection splices it is desirable to produce shunt to busbar lap splices with the lowest possible electrical resistance at cryogenic temperatures in order to maximise the current that can be transported safely through the shunts. The results presented here show that the solder bulk resistivity influences significantly the lap splice resistance in the transversal measurement configuration. Comparably low splice resistances are achieved with the low resistivity solders Sn96Ag4 and Sn60Pb40. The R_trans resistance of Sn77.2In20Ag2.8 soldered splices is about three times higher than that of the Sn60Pb40 and the Sn96Ag4 soldered ones.

For Sn96Ag4 and Sn60Pb40 soldered splices R_trans at 18 K can be estimated in reasonable approximation by dividing the RT resistance by a factor of 100. Thus, RT resistance measurements can be used to assess the shunt to busbar lap splice quality at LHC operating temperatures [16].

R_6 is determined by the Cu bulk resistance and only slightly influenced by the solder resistance (at 23 K: $R\_6_{Sn96Ag4}$=49.6±5.6 nΩ, $R\_6_{Sn60Pb40}$=49.5±6.4 nΩ, $R\_6_{Sn77.2In20Ag2.8}$=61.4±6.4 nΩ). An approximate fit of data points with Cu resistance ratios is possible. The R_6 ratio of Sn96Ag4 and Sn60Pb40 splices follows the resistance ratio of Cu with a RRR of about 300. Thus, the splice

resistance at cryogenic temperatures can be estimated from RT resistance measurements in R_6 configuration, provided that the RRR of the Cu splice profiles is known [17].

4.3. Butt splice resistance, resistance ratio and mechanical strength

The butt splice resistance measurements are sensitive to the influence of the Sn60Pb40 solder layer resistance over the entire temperature range from RT to below 20 K.

Good agreement is found between calculated and measured resistance values of the unsoldered Cu reference sample. For the soldered samples the measured resistance values are between 0.4-0.5 μΩ higher than the calculated resistance values, when only taking into account the Cu and Sn60Pb40 bulk resistance. This shows that the splice resistance is not only influenced by the bulk resistances.

The mechanical integrity of solder splices relies on the formation of intermetallic phases (Cu_3Sn and Cu_6Sn_5) between the metal items to be connected and the filler material (solder). These have a typical thickness in the order of 1 μm [18]. The resistance of these intermetallic layers, as well as constrictions of the current flow may have a measurable influence on the overall splice resistance [19] and cause the additional 0.4-0.5 μΩ splice resistance that is not explained by the bulk solder resistance.

Sn60Pb40 bulk solder is prone to creep, and its tensile strength depends strongly on the test speed and test temperature. At 20 °C the tensile strength of bulk Sn60Pb40 measured with a test speed of 20 mm/min and 1 mm/min is 50.0 MPa and 38.2 MPa, respectively [20]. Thus, the average tensile strength of the Sn60Pb40 soldered butt splices of about 80 MPa measured with a test speed of 2 mm/min significantly exceeds the tensile strength of the Sn60Pb40 bulk solder.

Such a difference between soldered butt joints and the bulk solder is expected and attributed to a constrained solder deformation by the base material. As an example, the tensile strength reported for Sn60Pb40 soldered butt joints at RT measured with a speed of 0.05 mm/min is 84 MPa [21].

Acknowledgements

In this work Christian Scheuerlein deserves the greatest thanks, for being a caring and always present supervisor during my time at CERN, and afterwards. His commitment can certainly serve as a reference. Also I would like to thank Professor Dr. rer. nat. Arno Förster from the Aachen University of Applied Sciences, for being the supervisor and first examiner of my work. A lot of people helped me with the set-up of the cryocooler experiment and during my stay at CERN in general. Many thanks go to the team of Building 927, represented by Jacky Mazet, for modifying countless parts to use in my setup. Gilles Trachez deserves gratitude for instructing me in the correct usage of "his" cryocooler setup and for providing assistance whenever needed. Without these ambitious people the progress of the experiment would not have been as smooth as it was. This also includes the help of the CERN Cryolab team, in particular Lionel Metral, who designed the sample holder, the heat shield and the vacuum vessel, and Friedrich Haug, who gave to me a lot of insight into the topic of cryogenics in general and was a great help during the performance evaluation of the cryocooler. Laetita Dufay-Chanat, also of TE-CRG, provided me with heater samples and a quick and easy way to attach them to the cryocooler setup. Amalia Ballarino, head of the TE-MSC-SCD section, aided in the design of the current leads and their thermalisation, certainly one of the challenging tasks at hand. I would furthermore like to thank Valerii Sytnik, for realising the data acquisition of my measurement signals. His work significantly boosted the quality of the data taken and the ease of the measurement process. In this context I would also like to mention Miguel Cerqueira Bastos, of the high-precision-measurement section, for borrowing me one of his HP multimeters for quite a while, and suggesting ways to improve the low-voltage measurements. I would like to thank Marc Pozzobon and the team of the Large Magnet Facility for sample production and Alexandre Gerardin from the CERN metallurgy laboratory for the tensile tests and the microscopic images he made. Ian Sexton invested quite some thought into the voltage taps, and prepared a convenient way to obtain signals from the samples. My colleague Simon Heck supplied me with hardness measurements of my samples and various other references and insights, not only limited to my work. Without my parents, I would never have gotten to this position. Thank You! I am grateful to my girlfriend Cagla, for supporting me in my decision to do this and during my stay away from Germany. Obrigado and gracias also to my Geneva crew and to Kati and Achintya.

References

[1] L. Evans (ed), “The Large Hadron Collider: A Marvel of Technology”, Lausanne/Boca Raton, FL : EPFL/CRC Press, 2009, ISBN 143980401X.

[2] P. Lee, D. Larbalestier, “Niobium-titanium superconducting wires: Nanostructures by extrusion and wire drawing”, Wire Journal International 36(2), 2003, 61-66.

[3] CERN, “The LHC Main Ring”, LHC Design Report Volume 1, Geneva, 2004, http://lhc.web.cern.ch/lhc/LHC-DesignReport.html, ISBN 92-9083-224-0.

[4] L. Belova, M. Genet, J.-L. Perinet-Marquet, P. Ivanov, C. Urpin, “Design and manufacture of the superconducting bus-bars for the LHC main magnets”, CERN LHC Project Report 540, Geneva, 2002.

[5] A. Jacquemod, A. Poncet, F. Schauf, B. Skoczen, J.Ph. Tock, “Inductive Soldering of the Junctions of the Main Superconducting Busbars of the LHC”, CERN LHC Project Report 698, Geneva, 2004.

[6] L. Rossi, “Superconductivity: its role, its success and its setbacks in the Large Hadron Collider of CERN”, Superconductor Science and Technology 23, 2010.

[7] P. Lebrun et al., “Report of the Task Force on the Incident of 19 September 2008 at the LHC”, CERN LHC Project Report 1168, March 31, 2009.

[8] A. P. Verweij et al., “Consolidation of the 13 kA Interconnects in the LHC for Operation at 7 TeV”, IEEE Transactions on Applied Superconductivity, Vol. 21, No. 3, June 2011.

[9] F. Bertinelli et al., “Towards a consolidation of LHC superconducting splices for 7 TeV Operation”, Proceedings of IPAC ’10, Kyoto, Japan, CERN-ATS-2010-144.

[10] Air Liquide, “Tetrafluoroethane-1,1,1,2 (R134A), C2H2F4, Physical properties, safety, MSDS, enthalpy, material compatibility, gas liquid equilibrium, density, viscosity, flammability, transport properties”, Gas Encyclopedia, Air Liquide Company Website, [Cited: September 26, 2011], http://encyclopedia.airliquide.com/Encyclopedia.asp?GasID=141.

[11] CTI-Cryogenics - Helix Technology Corporation, “Multiple uses of model 22C/350C Cryodyne refrigerators; Installation, operation and servicing instructions”, 1995, 8040272 Rev. B.

[12] T. Wikberg, “Multi-layer insulation (MLI) for magnet cryostats”, CERN Functional Specification, 1998, LHC-Q-ES-0002.00 rev. 1.0.

[13] S. Heck, C. Scheuerlein, P. Fessia, S. Triquet, A. Bonasia, “Resistivity of different solder alloys at cryogenic temperatures”, CERN TE-MSC Internal Note, 2011, EDMS No. 1133529.

[14] S. Heck, C. Scheuerlein, P. Fessia, R. Principe, “The RRR of the Cu components of the LHC main bus bar splices”, CERN TE-Note-2010-005, 2010, EDMS No. 1057918.

[15] D. R. Lide, “CRC Handbook of Chemistry and Physics 75th ed.”, Boca Raton: CRC Press, 1994: 12-41.

[16] S. Heck, C. Scheuerlein, G.P. Willering, “Room temperature resistance measurements for the quality control of shunt solder connections for the consolidation of the LHC main interconnection splices” CERN TE-Note-2010-34, EDMS Nr: 1097684, 2010.

[17] F. Bertinelli et al., “Production and Quality Assurance of Main Busbar Interconnection Splices during the LHC 2008-2009 Shutdown”, IEEE Trans. Appl. Supercond. 21, 2011, 1786-1790.

[18] D. M. Tench, “Oxidation of Solder Coatings”, The Mechanics of Solder Alloy Wetting & Spreading, edited by F.G. Yost, F.M. Hosking, D.R. Frear, Van Nostrand Reinhold, New York, 1993.

[19] C. Scheuerlein et al., “The effect of CuSn intermetallics on the interstrand contact resistance in LHC superconducting cables”, J. Appl. Phys. 97(3), 2005.

[20] K. Ring, “Reliability Issues with Leadfree Solders”, Zentrum für Verbindungstechnik in der Elektronik des Fraunhofer-IZM, ASTA Technology Company Website, [Cited: October 24, 2011], http://www.asta-technology.co.uk/documents/11.%20EMPS-2%20ZVE%20Lead%20Free(Karl%20RING).pdf.

[21] L. Quan, D. Frear, D. Grivas, J. W. Morris JR., “Tensile Behavior of Pb-Sn Solder/Cu Joints”, Journal of Electronic Materials, Vol. 16, No. 3, 1987.